FACULDADE DE ENGENHARIA DA UNIVERSIDADE DO PORTO

Investigation of the operating behaviour of a pyrolysis gas fuelled internal combustion engine

Afonso Guilherme Veloso Ribeiro dos Santos

Master in Mechanical Engineering
Fluids and Energy

Supervisor: Prof. Abel Ilah Rouboa

Supervisor: Prof. Karsten Wittek

September 30, 2025

Investigation of the operating behaviour of a pyrolysis gas fuelled internal combustion engine

Afonso Guilherme Veloso Ribeiro dos Santos

Master in Mechanical Engineering
Fluids and Energy

September 30, 2025

Resumo

A transição do setor energético para soluções de baixo carbono tem impulsionado o interesse por combustíveis alternativos para motores de combustão interna (MCI), especialmente aqueles capazes de reduzir as emissões de gases com efeito de estufa mantendo elevada eficiência operacional. Entre estes, o gás de pirólise, obtido pela decomposição térmica de biomassa e resíduos, constitui uma opção renovável e potencialmente neutra em carbono. A sua aplicabilidade em sistemas de produção combinada de calor e eletricidade (CHP), baseados em MCI, torna-o um candidato promissor para a geração estacionária de energia. O enriquecimento com hidrogénio do gás de pirólise melhora a estabilidade de combustão, a eficiência e o perfil de emissões, mitigando algumas das limitações associadas ao seu baixo poder calorífico inferior (PCI) e composição variável.

Esta dissertação apresenta o projeto, implementação e avaliação experimental de um MCI pesado adaptado para operar com gás de pirólise com diferentes teores de hidrogénio. O trabalho envolveu o desenvolvimento de um novo sistema de alimentação de combustível, combinando uma válvula proporcional e um distribuidor personalizado, em conjunto com modificações extensivas de software na unidade de controlo do motor (ECU). Foi conduzido um programa sistemático de ensaios utilizando hidrogénio puro, gás de pirólise enriquecido com hidrogénio baseado em composições de referência do Fraunhofer Institute e combustíveis alternativos convencionais, como biometano e biogás.

Os resultados demonstram que a operação com hidrogénio puro atingiu a maior eficiência térmica (até 39%) com emissões de NO_x praticamente nulas, enquanto o gás de pirólise enriquecido com hidrogénio apresentou desempenho semelhante, mas foi limitado por restrições de escoamento no distribuidor para misturas de baixo PCI. Os combustíveis ricos em metano alcançaram eficiências comparáveis, mas geraram emissões de NOx mais elevadas, que puderam ser mitigadas através da otimização da relação ar–combustível. O estudo confirma a viabilidade técnica da operação de MCI utilizando diversos combustíveis gasosos, mantendo alta eficiência e baixas emissões, e identifica melhorias de hardware como fator-chave para explorar plenamente o potencial do gás de pirólise em aplicações CHP e outras soluções de geração estacionária.

Palavras-chave: Gás de pirólise, Enriquecimento com hidrogénio, Motor de combustão interna, Combustíveis alternativos, CHP, Redução de emissões, Eficiência térmica.

Abstract

The transition of the energy sector towards low-carbon solutions is driving increased interest in alternative fuels for ICEs, particularly those capable of reducing greenhouse gas emissions while maintaining operational efficiency. Among these, pyrolysis gas, derived from the thermal decomposition of biomass and waste, offers a renewable and potentially carbon-neutral option. Its compatibility with existing infrastructure, particularly in combined heat and power applications, positions it as a potentially viable candidate for incorporation into stationary energy generation systems. Hydrogen enrichment of pyrolysis gas has been demonstrated to enhance combustion stability, efficiency, and emission characteristics, thereby addressing some of the limitations associated with its low heating value and variable composition.

The present dissertation is an exposition of the design, implementation, and experimental evaluation of a heavy-duty internal combustion engine (ICE) that has been adapted to operate on pyrolysis gas with varying hydrogen content. The work involved the development of a novel fuel delivery system, which incorporated a proportional valve and a custom distributor, in conjunction with extensive ECU software modifications. A systematic testing programme was conducted using pure hydrogen, hydrogen-enriched pyrolysis gas based on Fraunhofer Institute reference compositions, and conventional alternative fuels such as biomethane and biogas.

The findings indicate that pure hydrogen operation attained the highest thermal efficiency (up to 39%) with negligible NO_x emissions. In contrast, hydrogen-enriched pyrolysis gas exhibited comparable performance but was constrained by distributor flow limitations for low-LHV mixtures. Methane-rich fuels exhibited comparable efficiencies, yet they generated elevated NO_x emissions. This issue could be mitigated through the optimisation of the air-to-fuel ratio. The study confirms the technical feasibility of different fuel ICE operation while maintaining high efficiency and low emissions, and identifies hardware improvements as key to unlocking the full potential of pyrolysis gas in CHP and other stationary power applications.

Keywords: Pyrolysis gas, Hydrogen enrichment, Internal combustion engine, Alternative fuels, CHP, Emission reduction, Thermal efficiency.

UN Sustainable Development Goals

The United Nations Sustainable Development Goals (SDGs) provide a comprehensive global framework aimed at promoting a more equitable, inclusive, and sustainable future for all. Established in 2015, these 17 interrelated goals address a broad spectrum of critical global challenges, including poverty, inequality, climate change, environmental degradation, and the advancement of peace, justice, and strong institutions. The SDGs offer clear targets and actionable pathways for governments, businesses, and individuals to align their efforts towards fostering sustainable development. They emphasize the interconnectedness of economic growth, social inclusion, and environmental protection, ensuring that progress is made in a way that benefits both people and the planet.

In the context of this thesis, the SDGs serve as an essential framework for exploring and identifying sustainable solutions within the transportation and energy sectors. The transition to more sustainable energy sources, the adoption of cleaner technologies, and the reduction of carbon emissions are key challenges that align closely with the SDGs. The following SDGs are particularly relevant to this research, as they underscore the importance of advancing energy systems and infrastructure in a way that addresses environmental concerns and promotes long-term societal benefits. For each goal, specific contributions, performance indicators, and metrics will be discussed to measure progress and impact.

SDG 7 Ensure access to affordable, reliable, sustainable, and modern energy for all. This goal is central to promoting energy equity and supporting the transition to renewable energy sources such as syngas and hydrogen.

SDG 9 Build resilient infrastructure, promote inclusive and sustainable industrialization, and foster innovation. This goal focuses on the development of robust infrastructure, the integration of green technologies, and fostering innovation in sustainable industries, crucial for enhancing energy systems.

SDG 11 Make cities and human settlements inclusive, safe, resilient, and sustainable. Urbanization plays a key role in energy demand, and this SDG emphasizes the need for sustainable cities with smart transportation solutions and energy-efficient buildings.

SDG 12 Ensure sustainable consumption and production patterns. The circular economy and sustainable production are critical aspects of this goal, which promotes responsible consumption of energy and resources and reduces waste, aligning with the transition to sustainable fuel sources.

SDG 13 Take urgent action to combat climate change and its impacts. Addressing climate change is central to this research, as transitioning to cleaner energy sources, reducing carbon emissions from transportation and industrial sectors, and optimizing energy use are all crucial in mitigating climate change.

SDG 15 Protect, restore and promote the sustainable use of terrestrial ecosystems, sustainably manage forests, combat desertification, halt and reverse land degradation, and halt biodiversity loss. Sustainable land and resource management, including the use of biomass for syngas production, directly support this SDG by reducing the environmental impact of industrial processes.

SGD	Target	Contribution	Performance Indicators and Metrics
7	7.2	Research on using pyrolysis gas as an alternative fuel for internal combustion engines contributes to this goal by replacing fossil fuels with cleaner and renewable energy sources, such as organic waste and biomass.	Energy intensity; Energy efficiency; Percentage of renewable energy in the fuel mix; Energy conversion efficiency.
9	9.4	The adaptation of internal combustion engines to run on pyrolysis gas involves innovation and modernization of existing systems, promoting sustainability in the automotive and other sectors that rely on these engines.	Manufacturing Impact; Percentage reduction in resource usage; Cost-benefit ratio for retrofitting internal combustion engines.
11	11.6	The use of pyrolysis gas can help reduce pollutants emitted by fossil fuel-powered engines, improving air quality in urban areas and contributing to the sustainability of cities.	Reduction in Urban Air Pollution; Waste-to-energy ratio in cities; Air quality index improvements.
12	12.2	Pyrolysis gas, derived from organic waste and recyclable materials, offers a solution for waste management and reducing the consumption of non-renewable resources, fostering a more sustainable cycle of production and consumption.	Circular Economy Contribution; Resource Efficiency; Reduction in the carbon footprint of production processes; Amount of biomass used per unit of energy produced.
13	13.2	The conversion of internal combustion engines to use alternative gases such as pyrolysis gas directly contributes to reducing greenhouse gas emissions, helping mitigate climate change.	Carbon Intensity; Environmental Impact Score.
15	15.2	By promoting the use of biomass (the source of pyrolysis gas) and reducing reliance on fossil fuels, your research can contribute to the preservation of natural ecosystems and the promotion of more sustainable agricultural and waste management practices.	Sustainable Biomass Use; Sustainability of biomass sourcing.

Acknowledgements

I would like to express my deepest gratitude to all those who contributed to the completion of this thesis. In particular, I am especially thankful to the team at the *Kolbenmaschinen Labor*, Ulla, Thomas, Holger, Vitor, Geovanne, and Prof. Kasten Wittek, for their guidance, support, and for helping me to grow and learn.

I am also sincerely grateful to all my friends who shared this academic journey with me, from the first classes to the final stages, as well as to everyone I met during my time at FEUP, whose companionship and encouragement made the path more enjoyable.

A special thanks goes to those who made my free time in Germany truly memorable, especially Beatriz, Tobias and Veronika, whose energy and company brought another life to my stay abroad.

I would like to acknowledge two of my closest friends, João and Tomás, for their continuous support, patience, and friendship throughout the entire process.

Above all, I am profoundly grateful to my parents and my brother for their constant encouragement and unimaginable belief in me.

Afonso Santos

"Man does not create something without, in some way, it defining him. He is the reflection of what he builds."

Fyodor Dostoevsky

Contents

List of Figures

List of Tables

Nomenclature

Abbreviations

50%MFB	50% Mass Fraction Burned
Ar	Argon
ATDC	After Top Dead Center
BDC	Bottom Dead Center
BSFC	Brake Specific Fuel Consumption
BTDC	Before Top Dead Center
CH_4	Methane
CHP	Combined Heat and Power
CI	Compression Ignition
CO	Carbon Monoxide
CoV	Coefficient Of Variation
CO_2	Carbon Dioxide
dCA	Degrees Crank Angle
DI	Direct Injection
ECU	Eletronic Control Unit
EFI	Electronic Fuel Injection
EGR	Exhaust Gas Recirculation
EV	Electric Vehicles
H_2	Hydrogen
H_2O	Water
HC	Hydrocarbons
ICE	Internal Combustion Engine
IMEP	Indicated Mean Effective Pressure
LHV	Lower Heating Value
N_2	Nitrogen
NO_x	Nitrogen Oxides
PID	Piping and Instrumentation Diagram
PM	Particle Matter
POX	Partial Oxidation
RPM	Rotations Per Minute
SCR	Selective Catalytic Reduction
SFC	Specific Fuel Consumption
SI	Spark Ignition
SMR	Steam Methane reforming
Syngas	Synthesis Gas
TDC	Top Dead Center

VVT	Variable Valve Timing

Notation

c_p	Specific Heat at Constant Pressure	J/kg·K
c_v	Specific Heat at Constant Volume	J/kg·K
e_i	Energy Fraction	–
lhv_{fuel}	Lower Heating Value of a Fuel	MJ/kg
lhv_i	Lower Heating Value of a Constituent	MJ/kg
M_i	Molar Mass of a Constituent	kg/kmol
$\dot{m}_{fuel}$	Fuel Mass Flow	kg/s
P	Pressure	Pa
PE	Pollutant Emissions	kg/kWh
P_{down}	Pressure Downstream the Regulator	Pa
P_{up}	Pressure Upstream the Regulator	Pa
R	Universal Gas Constant	J/mol·K
T	Torque	Nm
T_{up}	Temperature Upstream the Regulator	K
V	Volume	m^3
V_{engine}	Engine Displacement	L
w_i	Massic Fraction	–
W_i	Indicated Work	J
W	Work	J
y_i	Volumetric Fraction	–
$\eta_{thermal}$	Thermal Efficiency	%
γ	Ratio of Specific Heats	–
λ	Air-Fuel Ratio	–
ρ	Specific Mass	kg/m^3

Chapter 1

Introduction

The present dissertation investigates the potential for converting internal combustion engines to run on pyrolysis gas. The introductory chapter explains the motivation for the work and its objectives. Thereafter, the dissertation's structure is presented to facilitate understanding.

1.1 Motivation

Since the inception of internal combustion engines (ICES) in the late 19th century, they have been central to transportation, industry, and energy production. The evolution of these engines has been a continuous process, driven by both societal needs and technological advancements. The progression from the early spark-ignition engines developed by Nikolaus Otto in 1876 to the more efficient and powerful compression-ignition engines introduced by Rudolf Diesel in 1892 highlights the ongoing development of technology in response to evolving demands for performance, efficiency, and sustainability [1].

In the contemporary context, as the global community seeks solutions to pressing issues such as energy consumption, environmental degradation, and climate change, ICES remain central to discussions of energy conversion and the adoption of alternative fuels. However, the growing awareness of fossil fuels' environmental impact, rising costs, and the push for energy sustainability have posed new challenges for the continued reliance on conventional ICES. Since the 1970s, concerns regarding air pollution, exacerbated by the oil crises, have led to significant efforts by manufacturers and policymakers to reduce emissions, improve fuel efficiency, and explore cleaner energy sources. Legislative measures such as the Clean Air Act in the United States and the Euro emission standards in Europe have been pivotal in driving the automotive industry toward substantial improvements in engine performance and a reduction in harmful emissions [1, 2]. Eventhoguh, from 1990 to 2019, CO_2 emissions around the globe increased from an annual value of 23 gigatons of CO_2 equivalent to 38 gigatons [3].

As these emissions remain a major concern, global leaders are calling for a reduction in carbon emissions. Politicians and policymakers are seeking sustainable development in the face of the widespread effects of climate change. At the same time, research topics are shifting towards achieving a carbon-neutral balance in the ICEs. In this topic, several fuels have been studied as possible solutions to this question, and they are called alternative fuels. These fuels can generally be divided into biofuels, hydrogen and synthetic fuels [4]. Among these fuels is pyrolysis gas, which is derived from the thermal decomposition of organic materials in an oxygen-deprived environment. The resulting gas, which is cleaner and potentially renewable, includes a mixture of hydrogen, carbon monoxide, and methane. Pyrolysis gas can be produced from a variety of waste materials, including biomass, plastics, and agricultural residues, making it an attractive option for reducing reliance on petroleum-based fuels while also addressing waste management challenges [5].

However, the use of pyrolysis gas as a fuel for internal combustion engines presents unique technical challenges. Notably, pyrolysis gas has a lower energy density compared to conventional fossil fuels, which impacts its efficiency in standard ICES. Additionally, the chemical properties of pyrolysis gas require modifications to the engine, particularly in terms of fuel injection systems and exhaust systems, to optimise performance and reduce emissions. As Tunér [6] explains, the adaptation of ICES to alternative fuels like pyrolysis gas requires significant changes to fuel injection strategies, as well as the development of robust combustion technologies to handle the variable energy content of the fuel. Despite these challenges, research continues to explore the feasibility of pyrolysis gas as a viable alternative to conventional fuels, with promising developments in engine technologies and fuel conversion processes [5].

The environmental impact of using alternative fuels is another key factor. Tunér [6] highlights the potential of alternative fuels, such as pyrolysis gas, to mitigate the adverse effects of conventional fuel use, such as greenhouse gas emissions and air pollution. However, Ahmad [2] also points out that the adaptation of engines to pyrolysis gas requires careful consideration of emissions control technologies to minimise harmful pollutants like nitrogen oxides (No_x) and particulate matter (PM). This makes the research into pyrolysis gas not only a technical challenge but also an environmental necessity.

1.2 Objectives

The project in which this dissertation is included is a collaboration between *Labor Kolbenmaschinen of Hochschule Heilbronn* and Fraunhofer Institute for Environmental, Safety and Energy Technology-UMSICHT (*Fraunhofer-Institut für Umwelt-, Sicherheits- und Energietechnik UMSICHT*), and DEUTZ Company, and is funded by the German Government.

The Fraunhofer UMSICHT Institute has carried out comprehensive research and experimental studies on the generation of pyrolysis gas using different types of bio-residues typically available in Germany, including materials like straw, digestate, and sewage sludge. Additionally, the filtering of syngas components based on their molecular size, enhancing the quality of the gas produced, was also studied.

The Piston Machine Laboratory (*Labor Kolbenmaschinen of Hochschule Heilbronn*), where this dissertation takes place, is tasked with converting a conventional heavy-duty engine to run on different pyrolysis gas compositions and evaluating their behaviour. During the engine adaptation process, the laboratory will focus on evaluating the changes in the combustion process and efficiency as a result of hydrogen enrichment in the pyrolysis gas.

This project is great opportunity to examine how a conventional engine can be prepared for a wide spectrum of pyrolysis gas compositions and how they influence key combustion characteristics, emissions, and overall engine performance. Given hydrogen's clean-burning properties, it is expected that higher hydrogen concentrations in pyrolysis gas will result in improved combustion efficiency, better flame stability, and a reduction in harmful emissions such as CO.

A preliminary version of the engine was previously developed and tested; however, during operation with low hydrogen content mixtures, several limitations became evident. Specifically, the fuel injection system was unable to deliver the required mass flow rate of the fuel mixture, which in turn restricted the engine's power output and operational flexibility. In response to these challenges, the present work focuses on the development of a second engine version, modifying both software and hardware. The overarching objective of this project is to establish a versatile engine platform capable of operating efficiently across a broad spectrum of gaseous fuels, ranging from pure hydrogen to syngas mixtures containing as little as 30% hydrogen by volume.

Beyond contributing to a deeper understanding of pyrolysis gas behaviour in ICES, this research will provide valuable insights into how an engine can be prepared for distinct fuels while maintaining high efficiency.

1.3 Structure

This dissertation is structured into seven essential chapters.

The first chapter, of which this section is a part, introduces the theme of the dissertation and the motivation behind the research while also presenting the document's structure.

In the second chapter, a comprehensive literature review is conducted to provide the reader with a progressive understanding of the topic. Beginning with fundamental engineering concepts, the discussion gradually builds in complexity, exploring relevant studies conducted by various authors and researchers. This structured approach not only offers a clear historical and technical perspective but also establishes the necessary foundation to contextualise the research developed in this dissertation.

The third chapter has the purpose of presenting previous work developed at the laboratory and which will have a direct influence on this study. Regarding its content, this chapter includes information from hardware specially developed for similar tests and progressively enhanced.

The fourth chapter presents the core development of this thesis, detailing both the hardware and software modifications implemented. It outlines the system architecture, describes the components introduced or adapted, and explains the control strategies developed to enable stable and flexible engine operation under varying fuel conditions.

The fifth chapter, titled Test Methodology, provides a detailed explanation of the experimental setup and test procedures used during the several early tests. This includes a comprehensive description of the hardware and software essential for data acquisition and analysis throughout the study. Additionally, all the tools utilised in the research are outlined, including those specifically developed or adapted for this study's unique requirements.

The Results and Discussion contain the main results obtained in the form of different types of plots, which are easy to compare to the results obtained from the previous engine version. Alongside, the discussion part includes the overall comparison of the outcome of the work regarding its comparison to other existing versions.

The Conclusions chapter is where the overall evaluation of the developed system is presented, with the main findings and performance outcomes being highlighted. Furthermore, potential future research directions are discussed, providing insight into further improvements and research opportunities.

Chapter 2

Literature Review

This chapter begins with a comprehensive overview of the operation of ICES and the methods used to evaluate its performance. Subsequently, a concise exposition of the notion of cogeneration is proffered, accompanied by a delineation of how this particular engine type can be integrated with it. Additionally, a detailed explanation of pyrolysis gas is provided, including its composition and the potential advantages of using it as a fuel in ICES. Finally, a brief discussion is presented on the enhancement of syngas with hydrogen, highlighting its specific applications and the improvements it can bring to engine performance and efficiency.

2.1 Internal Combustion Engines Design

ICE aims to convert the chemical energy of the fuel into useful mechanical work through its combustion. Various engine configurations can be employed, depending on factors such as the type of fuel used, the desired power output and the efficiency of the operating cycle [1]. However, certain fundamental design principles must be adhered to to ensure optimal performance and reliability, as outlined in the following sections.

2.1.1 Working Principles

ICE engines can be based on several thermodynamic cycles, being the two most commonly used being Otto and Diesel, also known as spark-ignition and compression-ignition, respectively. In addition, both of these engine types can operate on two fundamental working cycles, the two-stroke and four-stroke cycles. Most of the engines operate on a four-stroke cycle regime. Figure 2.1 presents the Pressure-Volume diagrams of both the Otto and Diesel cycles.

As can be seen, in the Ideal Otto cycle, there is an isentropic compression (1–2), an isentropic expansion (3–4) and two isobaric heat exchanges (2–3 and 1–4). In the Diesel cycle, all the processes are the same except for the isochoric heat exchange (2–3) instead of the isobaric process

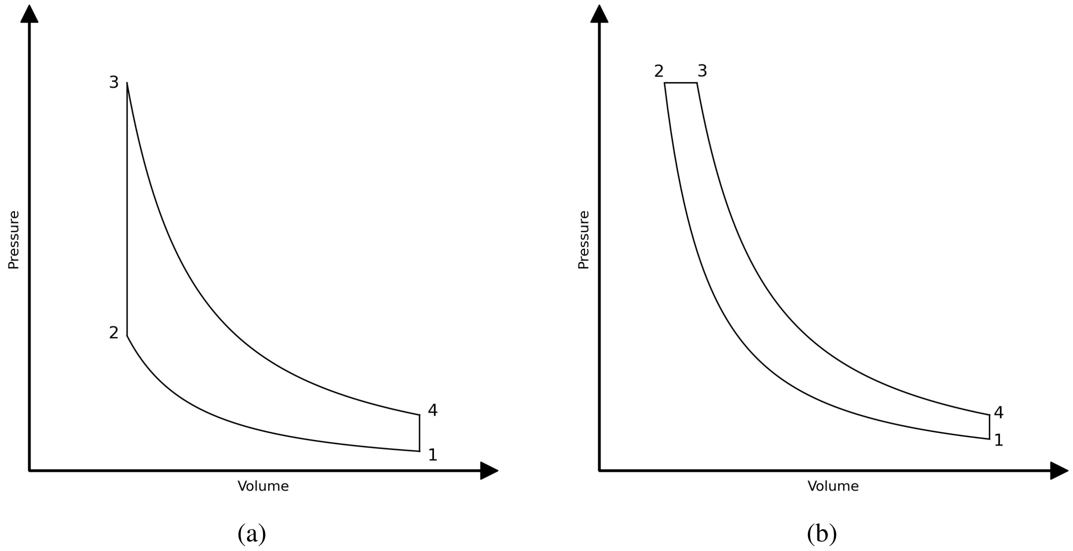

Figure 2.1: Pressure-Volume Diagrams for both: (a) Ideal Otto Thermodynamic Cycle and (b) Ideal Diesel Thermodynamic Cycle.

in the Otto cycle. Of course, these conditions are only possible in the ideal cycles and therefore engine manufacturers need to create engines capable of operating the close as possible to the ideal operating conditions.

The four-stroke engines in practice relay on physical strokes that can, generically, be described as below both for spark ignition (SI) and compression ignition (CI) engines.

1. Intake stroke – The intake valve opens, and the piston moves downward, towards BDC, drawing in air, in the case of CI engines, or a mixture of air and fuel, in SI engines.

2. Compression stroke – The intake valve closes, and the piston moves upward, towards TDC, to compress the air or air-fuel mixture. Compression increases the temperature and pressure of the mixture, preparing it for ignition.

3. Power stroke – In SI engines, just before the peak of compression, the spark plug ignites the air-fuel mixture, causing rapid combustion. In CI engines, just before the peak of compression, fuel is injected into the highly compressed air, causing it to ignite spontaneously. In both cases, the expanding gases force the piston downward, generating mechanical work.

4. Exhaust stroke – The exhaust valve opens, and the piston moves upward again to expel the combustion gases from the cylinder.

Regarding the differences between SI and CI engines, one of the most significant is the ignition method, while SI engines' ignition is obtained by a spark plug, in CI engines, ignition occurs spontaneously due to the high pressure and temperature in the cylinder [1]. This way, the compression ratio is notably higher in CI engines than in SI engines. CI engines typically operate with compression ratios between 14:1 and 25:1, while SI engines, on the other hand, use lower compression ratios, between 8:1 and 12:1, to avoid knocking, a phenomenon that can damage the engine when the fuel-air mixture ignites prematurely [1].

Another key difference lies in the fuel used. SI engines generally run on gasoline, which is a lighter fuel, and CI engines use diesel, a heavier fuel with a higher energy density. In terms of emissions, SI engines typically produce higher levels of CO and HC, but they generally emit lower levels of NO_x compared to CI engines, which produce more NO_x due to higher combustion temperatures [1]. CI engines also tend to emit PM, particularly in older models or under poor operating conditions.

In addition, CI engines offer higher torque at lower engine speeds, making them ideal for heavy-duty applications that require high efficiency under load, such as in trucks and industrial machinery. In contrast, SI engines are more suitable for applications requiring higher speeds, such as in passenger cars, where they offer smoother operation and faster throttle response [1].

2.1.2 Components

From the perspective of engine components, ICES are pretty similar to each other. Figure 2.2 represents a schematic of a generic four-stroke engine and resembles its main components.

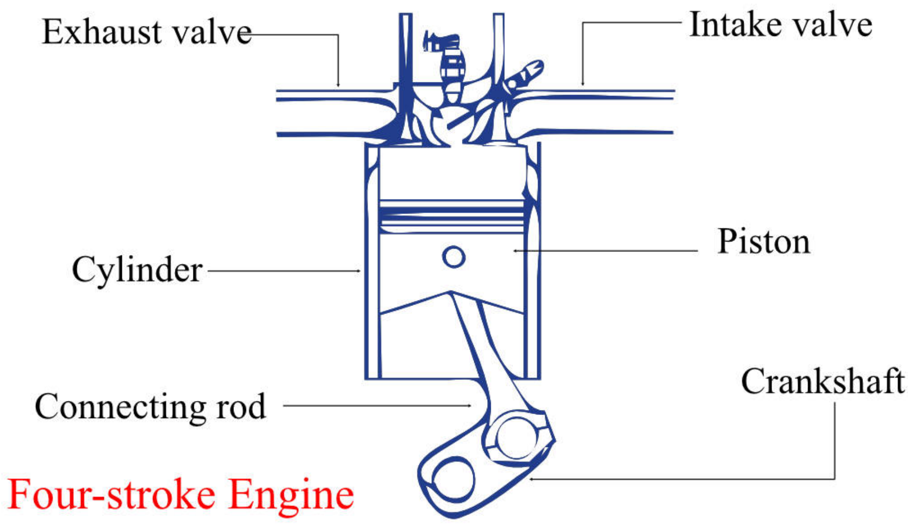

Figure 2.2: Generic four-stroke ICE [7].

The core of the engine is the cylinder, in which the air-fuel mixture is compressed and ignited. It is a key part of the engine block where combustion occurs. The size and shape of the cylinder are crucial factors that influence the engine's displacement, power output, and efficiency. Heywood [1] emphasises that the design of the cylinder head, which houses the intake and exhaust valves, is crucial for efficient airflow and combustion processes.

The piston, a moving component inside the cylinder, is responsible for converting the energy of the mechanical motion released during combustion. The piston moves up and down within the cylinder, and as Heywood [1] explains, the materials used in pistons are selected for their ability to withstand high temperatures and pressures while minimising weight.

The crankshaft is another critical component, responsible for converting the reciprocating motion of the piston into the rotational motion needed. The piston is connected to the crankshaft via the connecting rods, and during the power stroke, the combustion force is transmitted through the piston to the crankshaft, which converts the linear motion into rotational power. According to Heywood [1], the crankshaft must be designed to withstand high mechanical loads and efficiently transmit power from the piston to the rest of the engine.

The two primary types of valves in most internal combustion engines are the inlet (intake) valves and exhaust valves. The inlet valve controls the entry of the air or air-fuel mixture into the combustion chamber during the intake stroke. According to Heywood [1], the valve must remain open for a sufficient period to allow enough air or air-fuel mixture to enter the cylinder, but it must also close at the right moment to maintain optimal compression and combustion efficiency. The exhaust valve, on the other hand, governs the expulsion of exhaust gases from the combustion chamber after the fuel has been burned. During the exhaust stroke, the exhaust valve opens to allow the gases to exit the cylinder. Heywood [1] emphasises that the exhaust valve must open at the correct point in the engine cycle to allow effective expulsion of exhaust gases, while also preventing backflow into the combustion chamber. In an internal combustion engine, valve timing is controlled by the camshaft, which rotates in sync with the crankshaft. However, modern engines often employ variable valve timing (VVT) systems, which adjust the timing of the valve openings dynamically based on engine parameters. VVT improves engine efficiency across a wide range of operating conditions, optimising power output and reducing fuel consumption and emissions [1].

Alongside the previous, which are present in both SI and CI, the fuel injection and ignition systems differ slightly. Starting with the fuel injection system, its function is to deliver fuel to the combustion chamber in a fine mist or atomised spray. This atomization ensures that the fuel mixes thoroughly with the air in the combustion chamber, allowing for a more uniform and efficient combustion process. According to Heywood [1], the effectiveness of this atomization is influenced by factors such as injector design, fuel pressure, and injection timing. In SI engines, the fuel injection system injects the fuel directly into the intake manifold or, in more advanced configurations, directly into the combustion chamber (DI), opposed to older engines, in which carburettors were used to mix fuel with air before it entered the intake manifold. In CI engines, the fuel is injected directly into the combustion chamber at very high pressures. Heywood [1]explains that the high pressure is necessary to overcome the high compression within the chamber and to achieve the fine atomization needed for efficient combustion.

Something common to both SI and CI engines is that when running on fuels such as syngas or hydrogen, it may be necessary to design and implement a completely new fuel distribution and injection system. This is primarily because standard market injectors are not typically designed to handle the unique characteristics of these alternative fuels. Syngas and hydrogen have different physical properties compared to conventional fuels like gasoline or diesel, such as lower energy densities and different combustion characteristics, which means that standard injectors may not provide the required fuel flow rates.

According to Heywood [1], the exhaust system serves several key functions. The first and most obvious is to direct exhaust gases away from the engine, preventing the build-up of harmful pressure in the cylinders. The exhaust manifold collects exhaust gases from the cylinders and channels them to the rest of the exhaust system in the most efficient way, to prevent back pressure. One of the most significant parts of the exhaust system is the catalytic converter. Its function is reducing harmful emissions, particularly CO, NO_x, and HC, through chemical reactions that convert these pollutants into less harmful substances such as N_2, H_2O, and CO_2. The catalytic converter works by providing a substrate for catalysts, typically made of platinum, palladium, and rhodium, to promote these chemical reactions. Another key component is the muffler, which reduces the noise produced by the engine's exhaust gases. Heywood explains that the muffler works by using a series of perforated tubes and sound-absorbing materials to dissipate sound waves, thereby reducing the overall noise level emitted by the engine.

To increase the engine power output, two systems were created: these systems are turbochargers and superchargers, which are both forced induction systems. A turbocharger uses the engine's exhaust gases to spin a turbine, which drives a compressor that forces additional air into the engine. This method utilises waste energy from exhaust gases, making it more efficient in terms of power output per unit of fuel used. In contrast, a supercharger is mechanically driven by the engine via a belt connected to the crankshaft, which delivers instantaneous boost to the engine through the use of some of its power.

2.1.3 Performance and Key Parameters

The performance of an ICE is determined by a variety of factors that influence its ability to convert fuel into mechanical work. Key parameters that define engine performance include power output, torque, thermal and fuel efficiency, and particle emissions.

2.1.3.1 Power Output and Torque

Power output is the measure of the engine's ability to perform work, typically expressed in horsepower (HP) or kilowatt (kw). It is a function of torque, which is the twisting force generated by the engine, and engine speed (RPM), with the relationship described by the equation 2.1 [1].

$$W = \frac{T \cdot n}{9550} \tag{2.1}$$

Torque is expressed in Newton-meters (Nm) in the SI system, and it is measured using dynamometers based on the deflection of the rotating shaft. One example is an eddy brake, which measures the power output of an engine by applying a resistive load. It works by generating eddy currents within a conductor, which create opposing magnetic fields that resist the motion of the engine's rotating parts, converting mechanical energy into heat [8, 9].

2.1.3.2 Thermal Efficiency

Thermal efficiency is an important indicator of how well the engine converts the chemical energy in fuel into mechanical energy. It is a function of the engine's power and the fuel's mass flow and lower heating value (LHV). It can be calculated according to equation 2.2.

$$\eta_{thermal} = \frac{\dot{W}}{\dot{m}_{fuel} \cdot LHV_{fuel}} \cdot 100 \tag{2.2}$$

This value is typically low in conventional ICES due to losses in the form of heat, friction, and exhaust gases. Heywood [1] highlights that improving thermal efficiency involves optimising combustion processes, minimising friction losses, and recovering waste heat. For example, turbocharging can improve thermal efficiency by using exhaust gases to boost engine power without additional fuel consumption. Compression ratio, fuel mixture quality, and combustion timing are key factors influencing thermal efficiency. For conventional Otto engines, thermal efficiency typically ranges from 20% to 30%, while Diesel engines, on the other hand, generally exhibit higher thermal efficiency, typically between 30% and 40%, due to their higher compression ratio and more efficient combustion process [8].

2.1.3.3 Specific Fuel Consumption

Specific fuel consumption (SFC) is used to assess how much fuel is consumed per unit of power output, typically measured in grams per kilowatt-hour (g/kWh) as shown in equation 2.3.

$$SFC = \frac{\dot{m}_{fuel}}{\dot{W}} \tag{2.3}$$

It is an important metric in performance testing as it indicates how efficiently an engine uses fuel to generate power. SFC is commonly used to compare the efficiency of different engine types or fuels, such as gasoline, diesel, or alternative fuels like pyrolysis gas [8]. For Diesel engines, typical SFC values range from 190 to 230 g/kWh, which are relatively low compared to Otto engines, in which the SFC tends to range from 250 to 300 g/kWh, reflecting their lower efficiency compared to Diesel engines. For Syngas engines, SFC values can vary significantly based on syngas composition and operating conditions, but typically range from 300 to 350 g/kWh. The lower calorific value of syngas and its variable composition contribute to higher SFC values compared to conventional fuels.

2.1.3.4 Pollutant Emission

Pollutant emissions are a major concern in evaluating engine performance, especially in the context of environmental regulations. Common pollutants produced by ICES include CO, CO_2, NO_x, HC, and particulate matter (PM). This metric assesses the amount of a pollutant released per unit power produced, as equation 2.4 presents.

$$PE = \frac{\dot{m}_{pollutant}}{W} \tag{2.4}$$

Pollutant generation is assessed through exhaust gas analyser devices. Heywood [1] emphasises that exhaust gas recirculation (EGR), catalytic converters, and selective catalytic reduction (SCR) are essential technologies used to reduce emissions. The use of alternative fuels, such as syngas or hydrogen, can also lead to reduced CO, CO_2 and particulate emissions, although they may affect NO_x formation due to higher flame temperatures. According to the Euro 7 emissions legislation [10], which sets stricter limits for pollutants from new cars, the limits for NO_x are 60 mg/km for gasoline and 80 mg/km for diesel vehicles, while the limit for PM is 7 mg/km for most ICES.

2.1.3.5 Indicated Mean Effective Power

Indicated mean effective power or IMEP represents the average pressure in the combustion chamber over a complete engine cycle that would produce the same indicated work if it acted uniformly on the piston [1]. It is obtained by the division of the indicated work per cycle, W_i, by the engine displacement, V_{engine}, according to Equation 2.5.

$$IMEP = \frac{W_i}{V_{engine}} \tag{2.5}$$

W_i is obtained by the integration of the pressure over volume, while V_d is the engine's geometric displacement.

2.2 ICES in Combined Heat and Power Applications

Combined Heat and Power (CHP), or cogeneration, is an energy generation approach where electricity and useful thermal energy are produced simultaneously from a single fuel source. Unlike conventional power generation systems that discard thermal energy as waste, CHP systems recover this heat for productive use, significantly increasing leading to the system efficiency of the process, often reaching 70% to 90% [11]. A major advantage is the variability of the heat/electricity ratio, which can be optimised for the different applications in which they are used. Several energy conversion technologies can be used for cogeneration, among them are different types of turbines as steam, gas turbines, combined cycle gas and microturbines, reciprocating internal combustion engines, organic Rankine cycles, Stirling engines, and fuel cells [12].

Steam power plants are thermodynamically based on the Rankine cycle. The process is initiated by a heat source, most commonly a boiler, which converts pressurised water into high-pressure steam. In this process, water is initially pumped to a high pressure and subsequently heated to its corresponding boiling point. The water undergoes phase change to steam, and is often further superheated to temperatures above the saturation point to increase thermal efficiency. The high-energy steam that is the result of this process is directed through a multistage steam turbine, where it undergoes expansion and mechanical work is performed, thereby converting thermal energy into kinetic energy and reducing its pressure in the process [12].

The organic Rankine cycle (ORC) is predicated on the same principle as that of a steam turbine, albeit with the utilisation of an organic working fluid. The substance under consideration is a fluid (distinct from water) that possesses either a lower or higher boiling point [12].

Gas turbine systems are operated based on the Brayton thermodynamic cycle, which is extensively utilised in power generation applications. In this cycle, ambient air is drawn into a compressor and driven into the combustion chamber, where fuel is injected and burned at constant pressure, resulting in a high-temperature, high-energy gas stream. The hot gas is expanded through a turbine, passing through rows of vaned blades, creating rotation in them, thereby reducing its pressure back to atmospheric levels. The process of expansion drives the turbine rotor, which is mechanically coupled to the shaft of an electric generator. As the shaft rotates within a magnetic coil, it induces an electric current, generating electricity. Notwithstanding the prevalence of natural gas as the most utilised fuel, owing to its clean combustion characteristics and accessibility, alternative fuels such as fuel oil and diesel can also be employed. The power output of gas turbines is typically in the range of a few hundred kilowatts to several hundred megawatts, making them suitable for both decentralised energy production and large-scale power plants [12].

From a thermodynamic perspective, combined systems consist of two interconnected thermodynamic cycles operating at different temperature levels and linked through a common working fluid. In closed or indirect configurations, the working fluid – typically helium or air – circulates within a sealed loop, remaining isolated from the combustion process. The fluid is heated via a heat exchanger before expanding through a turbine to generate mechanical power. Following the process of expansion, the fluid is subjected to cooling, and the thermal energy that is extracted can be utilised for heating applications, thereby enhancing the overall efficiency of the system. In such systems, heat can be supplied by various sources, including the combustion of fossil or renewable fuels, as well as nuclear or solar thermal energy. When applied in Combined Cooling, Heating, and Power (CCHP) systems, this configuration can achieve overall fuel conversion efficiencies between 70% and 90%, with power-to-heat ratios typically ranging from 0.6 to 2 [12].

Reciprocating internal combustion engines are extensively utilised in both traction and stationary applications, functioning as primary power sources for mechanical systems or for driving electric generators. Reciprocating engines offer multiple opportunities for the recovery of waste heat, which significantly enhances their overall efficiency in CHP systems. The four primary sources of recoverable heat can be identified as exhaust gases, engine block cooling water, lubricating oil cooling water, and turbocharger cooling systems. The recovered thermal energy is typically available in the form of hot water or low-pressure steam, which is suitable for space heating, domestic hot water, or absorption cooling [12].

The dual-output capability of CHP not only maximises fuel utilisation but also reduces emissions and operational costs. ICE-based CHP units emerge as a practical and scalable solution for decentralised energy systems and industrial efficiency [13].

2.2.1 ICE Based CHP System Architecture

Figure 2.3 presents a generic ICE-based CHP system, in which the main components are highlighted.

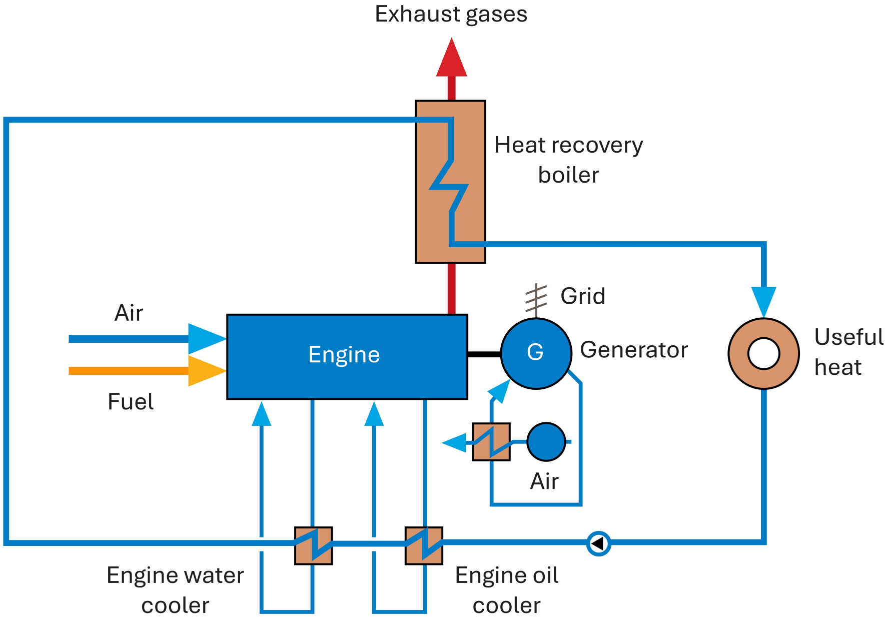

Figure 2.3: Generic ICE-based CHP system.

In this type of CHP system, the core component is the ICE, which is fed with air and fuel to convert the chemical energy into mechanical work. This mechanical energy is then transformed into electricity via a generator, which will be discussed in more detail in the following section.

Simultaneously, a substantial amount of heat is generated during the combustion process, primarily through the engine's exhaust gases and its cooling system. Instead of letting this thermal energy go to waste, the system employs heat exchangers, such as a heat recovery boiler, which captures the heat from the exhaust gases. The captured heat is then repurposed for useful energy applications.

Furthermore, additional heat exchangers are utilised for cooling the engine water and engine oil. These exchangers facilitate the efficient transfer of heat from the engine's fluid systems, ensuring optimal operation and prolonging the lifespan of the engine components. By maximising these heat exchange processes, the system can convert the waste heat into valuable thermal energy, which can be used for a wide range of heating applications, including industrial processes, district heating, and even domestic hot water production.

The integration of all the referred components enables the CHP unit to operate efficiently, achieving overall system efficiencies of up to 80% [14].

2.2.2 Electricity Generation

The electricity generated in a CHP system can be used for on-site consumption or exported to the grid, making these systems particularly valuable in both industrial and commercial applications. The efficiency and reliability of the electricity generation process are critical to the performance of CHP systems, and there are two main types of generators used for this purpose: synchronous generators and asynchronous/induction generators [15].

2.2.2.1 Synchronous Generators

A synchronous generator is the most common type of generator used in grid-connected CHP systems. The main operating characteristics of these generators are outlined below [16]:

- Constant Speed: The rotor speed of a synchronous generator is synchronised with the grid frequency, typically 50 Hz or 60 Hz, depending on the region [17];
- Power Factor Control: Synchronous generators can adjust the excitation of the rotor to control both real and reactive power. This capability is crucial in CHP systems, as it helps maintain grid stability by managing fluctuations in load and voltage [18];
- Grid Stability: By providing voltage regulation and frequency control, synchronous generators contribute to overall grid stability. They help maintain the electrical frequency and can supply reactive power when needed, ensuring that the grid remains stable and reliable [18].

Synchronous generators are particularly valued for their high efficiency, especially during steady-state operation. Their ability to provide both active and reactive power is a significant advantage, as it directly contributes to the stability of the electrical grid. By regulating voltage and maintaining a constant frequency, synchronous generators play an essential role in large-scale CHP installations connected to the grid. In these systems, they ensure stable and reliable electricity generation while supporting the grid's stability by compensating for power demand and supply fluctuations. This dual capability, of generating electricity and contributing to grid regulation, makes synchronous generators the preferred choice for larger, grid-connected CHP systems [19].

2.2.2.2 Asynchronous/Induction Generators

Induction generators, also known as asynchronous generators, are another option for generating electricity in CHP systems. The main operating characteristics of these generators are outlined below:

- Variable Speed: Induction generators operate at a speed that is slightly lower than the synchronous speed of the rotor. As the prime mover (such as an engine or turbine) drives the generator, it induces a current in the rotor, generating electricity [15];

- Grid Independence: While induction generators can be used in off-grid applications, they often require additional components, such as capacitors, to maintain voltage stability and correct the power factor [16];

- Less Power Factor Control: Unlike synchronous generators, induction generators have limited ability to control the power factor. To improve this, external reactive power compensation is typically needed [20].

Induction generators are simpler and less expensive than synchronous generators, making them an attractive option for certain applications. They are robust and reliable, particularly in standalone systems or situations where grid stability is not a primary concern. Additionally, induction generators are easier to maintain due to their fewer components, which simplifies their operation and reduces maintenance costs. These advantages make induction generators particularly suitable for smaller, off-grid CHP systems or in applications where simplicity and cost-effectiveness are priorities. They are commonly found in smaller industrial or agricultural settings, where large-scale grid connectivity is not necessary. In such settings, induction generators are ideal for standalone or isolated systems, where synchronisation with the grid is not required [20].

2.3 Syngas

Synthesis gas, or syngas, is a versatile fuel produced through the gasification of carbon-rich materials. Composed primarily of hydrogen (H_2), carbon monoxide (CO), and carbon dioxide (CO_2), with smaller amounts of methane (CH_4) and other gases, syngas has gained significant attention as an alternative energy source due to its potential to replace traditional fossil fuels in various applications. The conversion of ICES to run on syngas offers a promising pathway to reduce dependency on petroleum-based fuels while contributing to cleaner, more sustainable energy systems.

2.3.1 Composition and Properties

Syngas is obtained through gasification processes from a variety of feedstocks, such as biomass, urban and industrial residue and even organic residue. Its composition and, consequently, properties can vary depending on the feedstock and production method [21]. With this, a possible range for the volumetric composition of syngas is presented in Table 2.1.

Table 2.1: Syngas composition on volume percent basis [21]

Species	Min	Max
H_2	8,6	61,9
CO	22,3	55,4
CH_4	0,0	8,2
CO_2	1,6	30,0
N_2 + Ar	0,2	49,3
H_2O	0,0	39,8

With regard to energy content, syngas generally exhibits a lower heating value (LHV) in comparison to conventional fossil fuels such as gasoline or diesel. The lower heating value (LHV) of gasoline is approximately 33,600 MJ/m³, whereas that of diesel is approximately 35,800 MJ/m^3. However, syngas typically ranges between 5.02 and 12.57 MJ/m^3, depending on the feedstock and gasification parameters [21]. This decrease in energy density is primarily attributable to the composition of syngas, which consists of a substantial proportion of hydrogen (H_2) and carbon monoxide (CO), in addition to diluents such as nitrogen (N_2) or carbon dioxide (CO_2), particularly in air-blown gasification systems.

Notwithstanding this limitation, syngas remains an attractive alternative fuel, particularly for internal combustion engines (ICEs) and combined heat and power (CHP) systems, due to its favourable combustion characteristics. The hydrogen content of syngas facilitates rapid ignition and clean combustion, yielding water vapour as a by-product. This process results in reduced carbon dioxide (CO_2) emissions per unit of energy released when compared to traditional fossil fuels [22]. Consequently, syngas emerges as a compelling option in contexts that prioritise the reduction of greenhouse gas emissions and the enhancement of energy sustainability.

Nevertheless, the utilisation of syngas gives rise to technical challenges. The presence of carbon monoxide (CO), despite its status as a combustible component, gives rise to concerns regarding safety and emissions. Robust emission control strategies are therefore required, as CO combustion can promote the formation of nitrogen oxides (NO_x) due to higher flame temperatures. In the absence of adequate control, NO_x emissions have the potential to nullify a proportion of the environmental benefits associated with syngas, as evidenced by [23].

From a combustion standpoint, syngas exhibits a higher laminar flame speed than gasoline or diesel, primarily due to its hydrogen fraction. It has been demonstrated that this can enhance combustion stability at lean operating conditions. However, there is also an increased risk of pre-ignition and knock, especially in high-compression engines. In order to accommodate these characteristics, it is often necessary to make modifications to the engine design, including the optimisation of ignition timing, fuel injection strategies and compression ratios [24]. For instance, advanced ignition control and turbocharging can help maintain performance while taking full advantage of syngas's fast-burning nature.

2.3.2 Production

The most common methods for syngas production are gasification, steam methane reforming (SMR), partial oxidation (POX), and pyrolysis.

Gasification involves heating carbon-rich feedstocks such as biomass, coal, or waste in a controlled environment with limited oxygen or steam at high temperatures. This process breaks down the feedstock into a gas mixture of hydrogen and carbon monoxide, which can be used for power generation, fuel production, or chemical synthesis. Studies have shown that biomass gasification can produce syngas with varying hydrogen content, depending on the feedstock and processing conditions [25].

Steam methane reforming is primarily used to convert natural gas (methane) into syngas by reacting methane with steam at high temperatures (700°C–1,000°C). This process is widely used in industry for hydrogen production and syngas synthesis [26].

Partial oxidation involves reacting hydrocarbons with a limited amount of oxygen at high temperatures to produce syngas. This method is quicker than gasification and is used for feedstocks like methane, coal, and liquid fuels. Research has shown that POX can generate syngas with a high concentration of carbon monoxide and hydrogen, suitable for various industrial applications [27].

Pyrolysis is a thermal decomposition process where organic material is heated in the absence of oxygen, producing syngas, bio-oil, and charcoal. While this method typically produces a lower yield of syngas compared to gasification, it is particularly useful for waste-to-energy applications [28].

Before syngas can be utilised in the different applications, it must undergo an extensive cleaning process to remove contaminants that can damage equipment or reduce performance. Common impurities include tars, particulates, sulfur compounds, ammonia, and halogens. According to Lotfi et al. [29], tar removal remains one of the most critical challenges, especially in biomass-derived syngas, requiring a combination of primary methods such as cyclones and filters, and secondary treatments like catalytic reforming or thermal cracking. In particular, ceramic filters and hot gas filtration units are effective at operating at high temperatures, helping maintain energy efficiency during cleanup.

Krotki et al. [30] highlight that advanced systems often include multi-stage cleaning, where syngas is first filtered for particulates, followed by desulfurization units using zinc-based sorbents, and finally dry or wet scrubbers depending on downstream requirements. These measures not only improve the operational stability of internal combustion engines and turbines but also ensure regulatory compliance and extend component lifespan.

2.3.3 Hydrogen Enhancement

Through the years, many researchers have evaluated the potential of Hydrogen enrichment in syngas. A study by Zhao et al. [31] investigated the effect of hydrogen enrichment in syngas on the combustion performance of a gas turbine. The results showed that by increasing the hydrogen content in syngas, the combustion efficiency increased by up to 7% at various operating conditions, while improving flame stability and reducing ignition delays, leading to higher efficiency at lower temperatures [31]. Another study, published in Sustainability by Zhang et al. [32] found that increasing the hydrogen fraction in syngas reduced NO_x emissions by up to 25% and CO emissions by up to 40% compared to conventional syngas combustion. The hydrogen-enriched syngas achieved these results due to faster combustion and lower peak temperatures, which helped reduce the formation of NO_x [32].

In an experimental study by Bai et al. [26], they demonstrated that increasing hydrogen in syngas raised the lower heating value (LHV) of syngas by up to 12% at 20% hydrogen enrichment. This indicates that the addition of hydrogen improves the energy output of syngas, making it a more effective fuel source [26].

In an experimental study published by Liu et al. [27], it was shown that hydrogen-enriched syngas in an internal combustion engine increased power output by 5% compared to standard syngas without hydrogen. The study also observed that the engine's thermal efficiency improved by up to 8% at medium loads with a 20% hydrogen addition [27].

A study by Wang et al. [25] showed that a syngas blend with up to 30% hydrogen improved combustion stability in both spark ignition and compression ignition engines. The study also emphasised that adjusting the hydrogen content in syngas could provide a flexible solution for dual-fuel systems and help accommodate various feedstocks for syngas production [25].

2.3.4 Syngas in Cogeneration

Syngas has not yet established itself as a significant player in commercial fuel markets, in contrast to more standardised alternative fuels such as biomethane or hydrogen. This limitation is primarily attributable to its inherently variable composition, its dependence on diverse local feedstocks, and the absence of a unified infrastructure for its distribution, purification, and storage. Conversely, syngas is predominantly produced and consumed on-site, frequently at facilities dedicated to the thermochemical conversion of biomass, municipal solid waste, or agro-industrial residues. This decentralised production model is inherently congruent with combined heat and power (CHP) applications, wherein both electrical and thermal energy can be immediately utilised at the point of generation, thereby optimising system efficiency and energy autonomy.

Menin et al. [33] conducted a comprehensive assessment of a 225 kW decentralised biomass gasification combined heat and power (CHP) plant installed in the mountainous regions of Italy. The study demonstrated that, when integrated with thermal energy recovery systems, locally generated syngas can achieve electrical efficiencies ranging from 17% to 26%. This validates the suitability of such solutions even in economically constrained or off-grid environments.

In a complementary study, Desclaux and Pereira Jr. [34] explored the economic and environmental potential of residual biomass-based gasification plants, emphasising their capacity to reduce externalities – including emissions from open biomass burning – and to provide distributed power and heat for rural or agro-industrial regions. The findings of the present study serve to reinforce the strategic role of syngas-based combined heat and power (CHP) in achieving local energy resilience and environmental benefits.

This viewpoint is further substantiated by Salem et al. [35], who utilised computational modelling to investigate the potential of Scottish agricultural waste as a feedstock for syngas-fed CHP. The findings of the study suggest that optimal gasifier operation occurs with an equivalence ratio of 0.30–0.35 and a feedstock moisture content below 10%. The study confirmed that syngas with sufficient energy content can be reliably generated and used for CHP in remote or off-grid applications, especially in agricultural settings.

Chapter 3

State of Research

The research conducted by previous students who have worked on similar problems, all within the *Labor Kolbenmaschinen of Hochschule Heilbronn*, was a major starting point for this project. While some of these studies utilised different equipment and experimental parameters, their findings remain highly relevant, serving as a valuable foundation for the work being developed in this dissertation.

Over the past years, the *Labor Kolbenmaschinen* has focused extensively on the use of alternative fuels in ICEs, fostering significant advancements in instrumentation, component design, data analysis, and experimental procedures. Through this research, a solid framework has been established, enabling continuous refinement of testing methodologies and analytical approaches. The insights gained from these studies directly support the current research, ensuring it builds upon well-established experimental knowledge while addressing new challenges in the field.

3.1 Gas Mixing Unit

The gas was simulated using a combination of H_2, CO, CO_2, and N_2 from high-purity (>99,999%) compressed gas cylinders, at 300 bar. Commonly, to create gas mixtures and regulate their compositions, mass flow meters are used. The downside of this type of system is the delay in the values read by the flow meters, making the system unreliable for transient operation. The design philosophy of this unit was for it to be a cheap and reliable system, and therefore, it was made from scratch. Since the system is only used with gases, it is possible to take advantage of their compressible properties.

The design principle of the system is based on the occurrence of supercritical flows, which are only dependent on the gas properties upstream of the orifice, and therefore, the measurements are more reliable. This way, the mass flow rate can be described by Equation 3.1 [36].

$$\dot{m}_{th} = A\sqrt{2p_1\rho_1}\sqrt{\frac{k}{k-1}\left[\frac{p_1}{p_2}^{2/k} - \frac{p_1}{p_2}^{\frac{k+1}{k}}\right]} \tag{3.1}$$

Considering two points, 1 and 2, upstream and downstream of an orifice, respectively, gas mass flow is dependent on the values of pressure, p_1 and p_2, and density, ρ_1. Additionally, the mass flow also depends on the cross-sectional area of the exit, A, and the isentropic index of the gas, k.

The second root in Equation 3.1 is only dependent on the pressure ratio, the relation between pressure downstream and upstream of the orifice, and the isentropic index. This way, the outflow isentropic function can be written according to Equation 3.2.

$$\Psi_s = \sqrt{\frac{k}{k-1}\left[\frac{p_1}{p_2}^{2/k} - \frac{p_1}{p_2}^{\frac{k+1}{k}}\right]} \tag{3.2}$$

Combining Equations 3.1 and 3.2, Equation 3.3 is obtained.

$$\dot{m}_{th} = A\sqrt{2p_1\rho_1}\Psi_s \tag{3.3}$$

Its maximum value is referred as Ψ_{max} [36] and, for this value, the flow becomes supersonic [37]. Experimental results have shown that when the pressure ratio falls below the critical threshold, the mass flow becomes independent of the downstream pressure and remains constant [36]. For higher pressure ratios than the critical one, an inverse parabolic shape is obtained as shown in Figure 3.1.

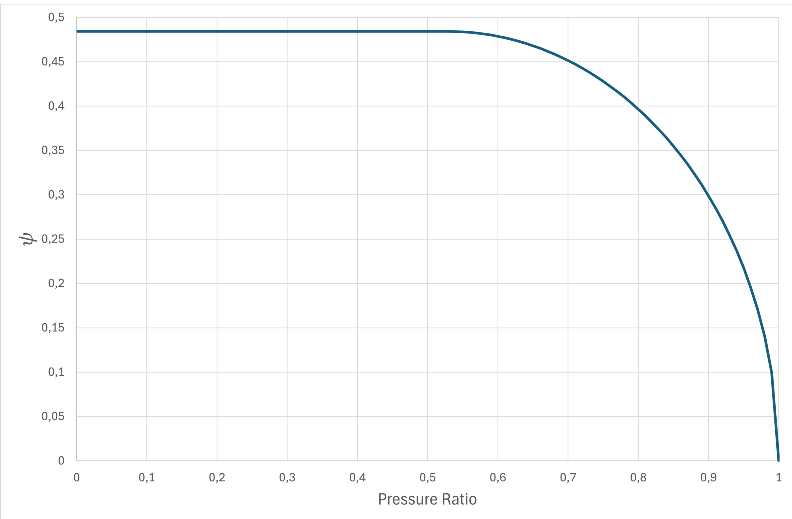

Figure 3.1: Ψ function variation with the pressure ratio.

The pressure ratio at which the outlet cross-section becomes choked and the mass flow ceases to vary is defined as the critical pressure ratio, expressed in Equation 3.4. The corresponding maximum dimensionless mass flow, denoted as Ψ_{max}, is calculated using Equation 3.5.

$$\left[\frac{p_2}{p_1}\right]_{crit} = \left[\frac{2}{k+1}\right]^{\frac{k}{k-1}} \tag{3.4}$$

$$\Psi_{\max} = \left(\frac{2}{k+1}\right)^{\frac{k}{k-1}} \sqrt{\frac{k}{k+1}} \tag{3.5}$$

By establishing a pressure differential in a compressible flow across an exit orifice, and ensuring that the pressure ratio remains below the critical threshold, a constant and measurable mass flow can be achieved—provided the cross-sectional area of the exit is known. This principle forms the foundation of the gas mixing system's design. For the gases used in this study, the critical pressure ratio is comprehended between 0,53 and 0,55, corresponding to (ψ_s) values between 0,47 and 0,48. This way, and considering, most of the work is developed in such conditions that the mass flow is supercritical, the (ψ_s) value of 0,48 was considered for the calculations.

The gas mixer unit contains a pressure regulator, adjusting the pressure downstream to 30 bar, a shut-off valve, a section with an orifice to create the isentropic outflow section, a mixing pipe and a 100 L settling tank. Due to the high variability in the fuel consumption by the engine, it was needed to have a buffer tank in the system in order to stabilise pressure oscillations and ensure the gas is mixed homogeneously. This way, the tank was filled until the working pressure, about 12 bar, and then emptied until the minimum operative pressure, 8 bar, as described in the pressure over time graphic. A pipe and instrumentation diagram from the experimental setup is presented in Figure 3.2, highlighting the main components of the system.

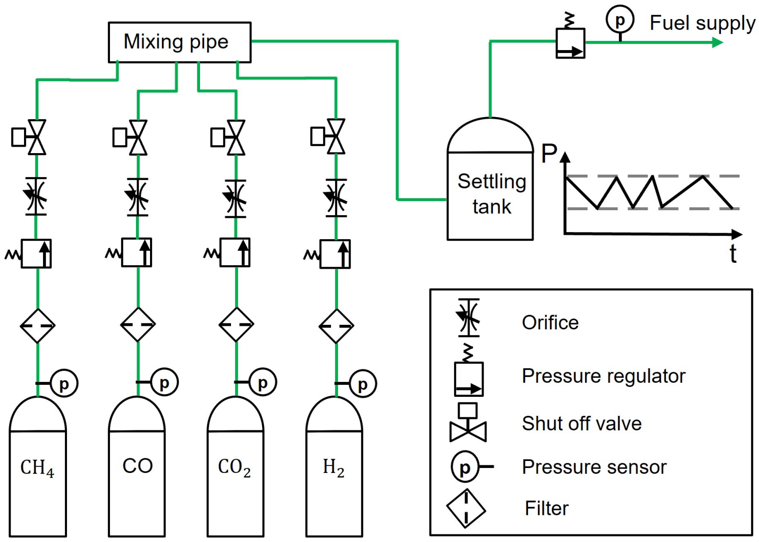

Figure 3.2: Gas mixing unit diagram.

The performance of the gas mixing unit has previously been assessed, with promising results obtained for the mixtures created, in comparison to the idealised models. The only minor issue identified pertained to the challenge in attaining the desired level of CO_2 in conditions of reduced ambient temperature.

3.2 Fuel Distributor

Over the years, multiple iterations of fuel supply systems have been designed, constructed, patented, and extensively tested, evolving through various technological approaches. These range from minor adaptations of existing commercial fuel injectors to the implementation of pneumatic and hydraulic actuator systems, culminating in fully mechanical actuation systems. In parallel, numerous experimental studies have been conducted to assess and refine the system's operational efficiency under a wide range of conditions, ensuring its adaptability and effectiveness in alternative fuel applications.

The latest design has undergone incremental refinements throughout successive projects, incorporating improvements based on experimental findings. The idea behind this design is to remove the fuel injectors, as they are the main limiter in terms of maximum fuel flow to the cylinders. This approach yielded a straightforward mechanical solution for the fuel supply, as illustrated in Figure 3.3.

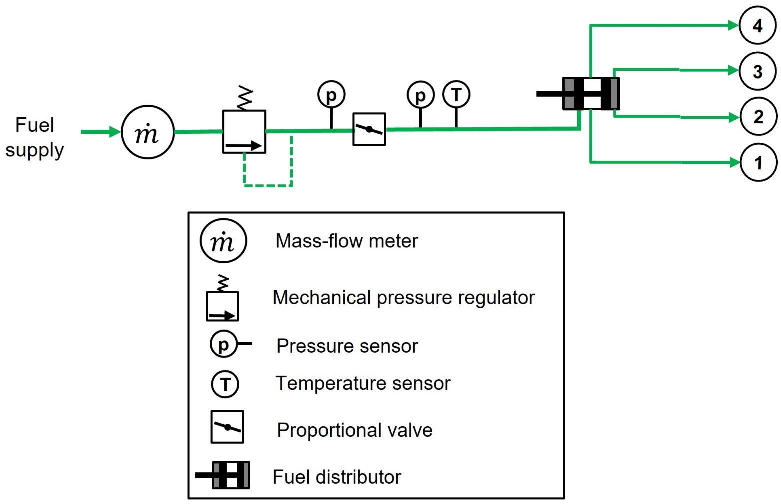

Figure 3.3: Fuel supply line diagram.

This diagram offers an overview of the key components integrated into the fuel supply system. The most critical element is the fuel distributor piece, which is preceded by pressure and temperature sensors. Before the sensors, a proportional valve is placed after another pressure sensor. This last sensor is positioned downstream of a mechanical pressure regulator that ensures the correct pressure levels before fuel enters the injection system. Upstream of this mechanical pressure regulator, there is a Coriolis flow meter in order to verify the mass flow calculated by the engine control unit.

The need for the mechanical pressure regulator arises from the design constraints of the distributor, which requires precise flow control to maintain stable and efficient engine operation. The distributor is a composition of several shafts, gears, springs and specially designed pieces to direct the hydrogen flow. Regarding the distributor main body, it can be seen in Figure 3.4 and more detailed in Appendix A.

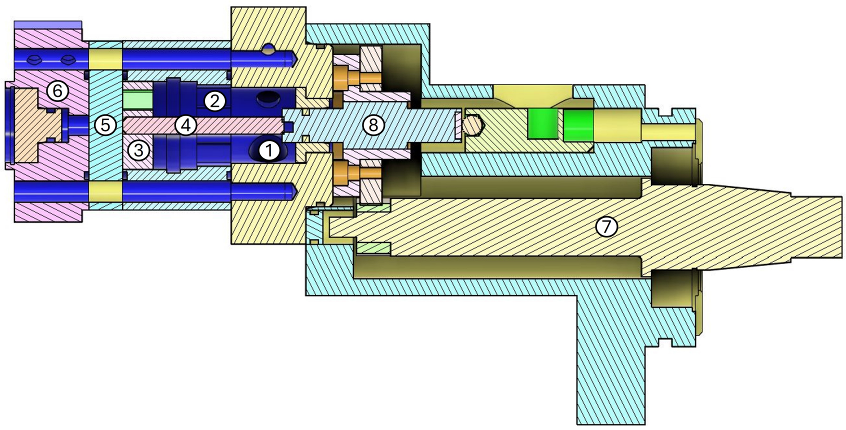

Figure 3.4: Distributor cut-view.

The fuel is introduced at (1), flowing to the chamber (2). Once this chamber is filled with fuel and pressurised, the flow will pass through the cut in component (3), which is rotating driven by the shaft (4). As plate (5) is static and features four cuts, one for each cylinder, as soon as the overlap of the cut from pieces (3) and (5) occurs, the flow passes by and moves towards component (6). In here, the flow is directed to a hose which is connected to each cylinder.

In terms of the kinematics of the system, the distributor's main gear rotates at half the speed of the crankshaft, which matches the fact that one power stroke occurs for every two rotations of the crankshaft. This rotational motion is transmitted, firstly to the shaft (7), then through the gear system to a shaft (8) which is connected directly to shaft (4). Regarding the graphite disk and steel plate, components (3) and (5), they are represented, respectively, in Figures 3.5a and 3.5b. The steel plate features four trapezoidal-section cuts extending through their entire axial length, one connected to each engine cylinder, while the graphite disk only features one cut. The movement from the graphite disk, resulting in the overlap of the cut sections, is what creates the flow.

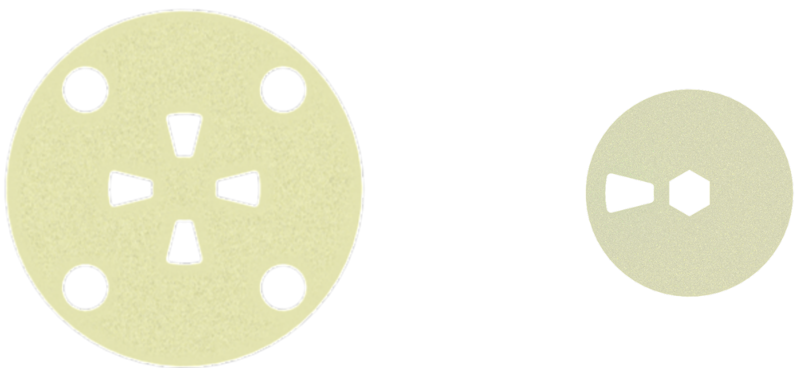

(a) (b)

Figure 3.5: Distributor overlapping plates: (a) Steel plate, (b) Graphite plate.

The design objective is to achieve precise control over the intake stroke utilising meticulous regulation of the mass of fuel admitted into the cylinder. In order to accomplish this, a calibration procedure was implemented in order to establish a reliable relationship between the downstream pressure of the pressure regulator and the corresponding fuel mass flow. All calibration and flow calculations are based on the assumption of supercritical flow through both the proportional valve and the fuel distributor, applying the theoretical framework and equations detailed in Section 3.1. These assumptions, although idealised, were validated through experimental testing carried out in previous projects with similar configurations, confirming their suitability for the present design.

Chapter 4

Engine Modifications

The engine utilised in this project had previously undergone extensive testing with various syngas compositions. These tests revealed a critical limitation: for syngas mixtures with lower heating values, the existing injection system was unable to deliver the required fuel mass flow into the combustion chamber. This inherent limitation subsequently constrained the engine's power output and operational versatility. Consequently, the development of a wholly novel fuel injection system for this engine was initiated.

In addition to the hardware modifications required to implement the new system, further software development was necessary to ensure proper integration and real-time control during engine operation. A new control strategy was designed that took into account the specificity of the updated fuel injection components geometries. This strategy was then transposed into the ECU software by implementing new control logic to guarantee stable and efficient engine performance under all operating conditions.

4.1 Hardware

The base characteristics of the engine used for this study, and which were the base for the hardware dimensioning, are presented in Table 4.1.

Table 4.1: Engine charateristics

Base engine model	DEUTZ TCD 3,6 L4
Number of cylinders	4
Bore x stroke	98 mm x 120 mm
Displacement	3621 cm^3
Compression ratio	17,2
Maximum brake power output	100 kW @ 2300 rpm
Maximum torque output	500 Nm @ 1600 rpm

The design of the new fuel supply system followed the architecture presented in Section 3.2. While some components had already been manufactured in earlier project phases and were available for reuse, others required modifications or redesigns to meet the current setup's specific objectives. Of all the components, the proportional valve was the most critical and the most technically demanding in terms of adaptation (see Figure 4.1). This valve plays a central role in regulating the mass flow of fuel injected into the engine, and its performance directly affects the precision and responsiveness of the entire fuel delivery system. Therefore, several mechanical adjustments and extensive calibration tests were performed to ensure that its operating characteristics matched the requirements of the new control strategy.

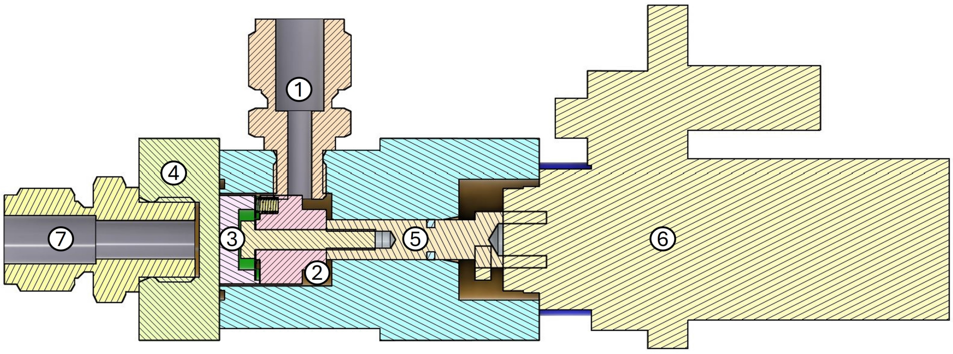

Figure 4.1: Proportional valve cut-view.

In this component, the fuel enters through a pressurised line onto port (1) and is directed into chamber (2), filling and pressuring it. The regulation of flow is accomplished through the modulation of the overlap between a movable graphite disk (3) and a fixed steel seat (4), thereby effectively varying the flow cross-section. The motion of the graphite disk is actuated via a shaft (5), which is directly coupled to an electric motor (6) responsible for precise positioning. After the implementation of the regulation, the fuel exits the valve through port (7) and is directed to the engine supply system, where it is subsequently conducted into each cylinder intake.

To dimension the proportional valve area needed, the fuel considered for the purpose was the base fuel provided by the Fraunhofer Institute, whose properties are detailed in Appendix B. The choice of this fuel as reference had to due with the fact of it being the fuel with the lowest LHV amongst the ones chosen for testing. To evaluate the mass of fuel needed for the design conditions, the values presented in the Table 4.2 were considered.

Table 4.2: Fuel calculation parameters

Parameter	Unit	Value
Engine power	kW	85
Efficiency	-	0,35
Fuel LHV	MJ/kg	12,11

As previously shown, the engine had a power output capability of 100 kW at 2300 rpm. Being this engine now used for asynchronous generation, it was prepared to run at 1500 rpm constant speed, so the maximum power output was adjusted for this speed while maintaining some operational margin. The values presented resulted in a mass flow of 62,76 Kg/h, which was equivalent to 348,68 mg of fuel per combustion cycle (cc), for an engine speed of 1500 rpm and a 4-cylinder engine. To dimension the new graphite disk, having the value for the fuel burned per combustion cycle, Equation 3.3 was used. The values considered for the several members of the equation are presented in Table 4.3.

Table 4.3: Graphite disk design parameters

Parameter	Unit	Value
Fuel density	kg/m^3	1,02
Flow function constant	-	0,48
Supply pressure	kPa	1200
Fuel mass flow	kg/s	$1,7 \cdot 10^{-2}$

The obtained value for the effective flow area was 7,30 mm^2 for the maximum load scenario. As a precautionary measure, an area of 8,00 mm^2 was adopted in the final design to incorporate a safety margin, ensuring reliable operation across a wider range of conditions.

This increase accounts for potential variations in manufacturing tolerances, uncertainties in syngas composition, and minor flow instabilities that may occur during transient engine operation. The slightly oversized design ensures that the fuel system remains capable of delivering the required mass flow even under less-than-ideal conditions. The updated component CAD model is displayed in Figure 4.2. For further detail, the technical drawing is included in Appendix A.

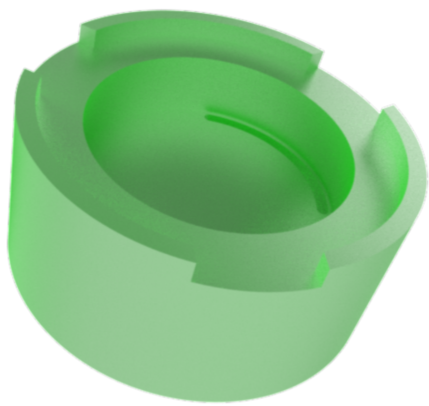

Figure 4.2: Graphite disk CAD model.

4.2 Software

The introduction of new hardware necessitated a comprehensive reconfiguration of the engine control strategy, which is managed by the ECU. A full software rework was necessary to accommodate the altered dynamics of the upgraded fuel delivery system.

In this project, a Trijekt ECU, specifically designed for ICES running on gaseous fuels, was chosen for its robust capabilities in engine management and fuel control. In this setup, the fuel flow is directly influenced by the valve's position, which is dynamically adjusted by the ECU. The software is responsible for calculating the fuel mass flow, considering key inputs such as valve position, engine speed, and fuel supply pressure. The process for determining the fuel mass flow, which served as the base for the software, is illustrated in Figure 4.3, where the relationship between these inputs and the mass flow is defined.

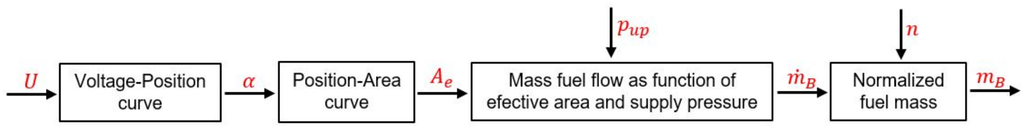

Figure 4.3: Fuel mass calculation process.

A digital signal from the proportional valve (U) corresponds to the valve's opening angle (α). This opening angle is can be translated into an effective flow area (A_e) using a pre-calibrated curve. Once the effective area of the flow path (A_e) is determined, the mass flow ($\dot{m}_B$) is calculated using equations 3.2 and 3.3. In this last equation, pressure values upstream (P_{up}) and downstream (P_{down}) the valve are considered. The resulting mass flow is subsequently converted to mass per cylinder per cycle (m_B) through equation 4.1, which is used as a variable in the generic operating engine maps.

$$m_B = \frac{\dot{m}_B}{z \cdot \frac{n}{2}} \tag{4.1}$$

In this Equation, z stands for the number of cylinders in the engine, while n stands for the engine speed. Since this engine is a four-stroke engine, there is only one combustion cycle per two revolutions of the engine. This creates the necessity to divide the engine speed by two. By using this detailed approach, the fuel mass flow can be accurately calculated, making some assumptions. The first one is the values considered for the reference pressure and temperatures of the atmosphere, according to DIN 1343. The second assumption is the constant value of the specific heat ratio in the operating range of temperatures and pressures. Lastly, since the flow through the proportional valve is a compressible flow, the same assumptions made for the gas mixing unit design were used.

Having the software architecture defined, the next step is implementing it. The resulting software menu is presented in Figure 4.4.

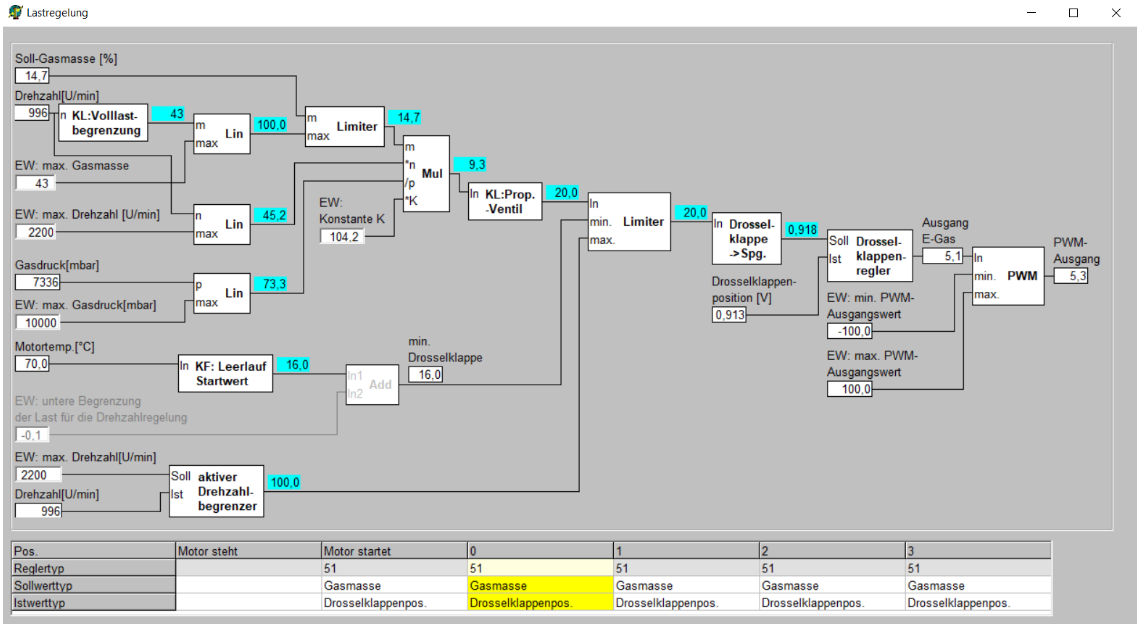

Figure 4.4: Software structure.

As can be seen, the proportional valve position is controlled by an engine map (*KN:Prop.ventil*) which converts calculated area to opening angle. For the area calculation, four parameters are needed. The first parameter is the constant k (*EW: Konstante K*), the other three are all normalised values and are referent to fuel mass (m), engine speed (n) and fuel supply pressure (p).

To obtain the value for the fuel mass demanded, there is a throttle pedal demand (*Soll-Gasmasse* [%]) resulting from an analogue input converted to a digital signal. This signal is passed through a limiter, which relates the engine speed (*Drezhal* [U/min]) to maximum fuel supply, through an engine map (*KN:Volllastbegrenzung*). In addition to the values on the map, the reference maximum value needs to be set independently (*EW: max. Gasmasse*). A reference value is set as the maximum engine speed (*EW: max. Drezhal* [U/min]) used to normalise the engine speed. For the fuel supply pressure, it is also necessary to define a maximum value (*EW: max. Gasdruck* [mbar]).

Some additional features were implemented for the control of the proportional valve. This way, after the value for the valve opening being determined it is passed through a limiter. In this limiter, the minimum value is obtained from an engine map relating the engine temperature (*Motortemp.* [ºC]) and the valve opening to sustain engine idle. The maximum value is obtained from the engine speed control system (*aktiver Drezahlbegrenzer*), which uses a PID controller to control the valve through the engine speed and maximum engine speed (*EW: max. Drezahl* [U/min]) inputs.

After passing the limiter, the value is converted from digital to analogue signal (*Drosselklappe->Spg.*), which is then compared to the signal being read from the throttle body (*Drosselklappenpo-*

sition [V]) by the ECU, creating a feedback loop (*Drosselklappenregler*). Before being converted into a Pulse Width Modulation signal, the control output generated by the ECU (*Ausgang E-Gas*) passes through an intermediate processing block to adjust the control signal to the appropriate format and scaling required (*PWMAusgang*).

Another important parameter controlled by the ECU is the spark timing, which is responsible for the electric discharge that ignites the fuel. For this, the engine map presented in Figure 4.5 was used.

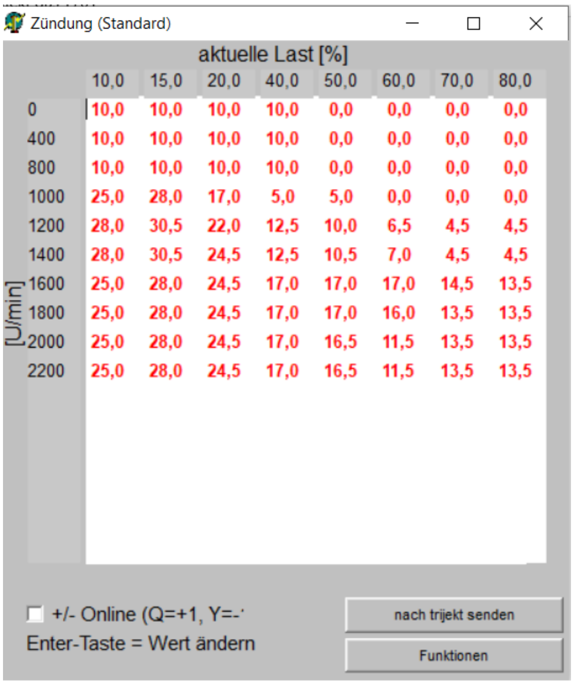
Zündung (Standard)

aktuelle Last [%]

[U/min]	10,0	15,0	20,0	40,0	50,0	60,0	70,0	80,0
0	10,0	10,0	10,0	10,0	0,0	0,0	0,0	0,0
400	10,0	10,0	10,0	10,0	0,0	0,0	0,0	0,0
800	10,0	10,0	10,0	10,0	0,0	0,0	0,0	0,0
1000	25,0	28,0	17,0	5,0	5,0	0,0	0,0	0,0
1200	28,0	30,5	22,0	12,5	10,0	6,5	4,5	4,5
1400	28,0	30,5	24,5	12,5	10,5	7,0	4,5	4,5
1600	25,0	28,0	24,5	17,0	17,0	17,0	14,5	13,5
1800	25,0	28,0	24,5	17,0	17,0	16,0	13,5	13,5
2000	25,0	28,0	24,5	17,0	16,5	11,5	13,5	13,5
2200	25,0	28,0	24,5	17,0	16,5	11,5	13,5	13,5

+/- Online (Q=+1, Y=-'

Enter-Taste = Wert ändern

nach trijekt senden

Funktionen

Figure 4.5: Spark timing map.

This map is a biaxial table relating the engine speed, in rpm, and the valve position, named as *aktuelle Last* [%]), to correspond to the spark timing in degrees crank angle before top dead centre (dCA BTDC). Due to the limited number of columns in the table, the maximum load represented on the map was 80%. In these cases, the ECU uses the last known value, corresponding to the 80% load column, and keeps it constant for loads higher than this, which can be considered an accurate estimate, as combustion behaviour does not change significantly within this range. The downside of this part of the software is the need for updating the map every time the fuel is changed, since the software does not allow for storing several ignition maps, as other high-end ECUs allow.

Apart from the steady state and stable operation, which was already ensured by the ECU according to the base calibration, there are some other potentialities to be explored. Trijekt ECU software provides the flexibility to configure multiple operational stages, each tailored to a specific mode of engine operation. These stages include:

- Starting Phase – Controls fuel delivery to guarantee a smooth and stable engine startup while avoiding overfilling the engine with fuel.

- Idle Control – Manages minimal fuel injection and adjusts ignition timing to maintain steady operation at low, constant and stable speeds.
- Speed Control – Adjusts fuel injection and ignition timing to sustain the desired engine speed.

The engine operates efficiently across a wide range of conditions thanks to its own set of control strategies and parameter sets for each operational stage. Unfortunately, the operator can only trigger a transition between stages manually via the Trijekt software interface since no other form of communication is supported yet.

The Starting Phase mode is the only exception to the rule, as it does not need any operator intervention to enter or exit this mode. As soon as the engine speed is detected to be above 200 rpm, this mode is engaged and is only disengaged when the engine speed is detected above 800 rpm. In this mode, the purpose is for the operation to be simplified, resulting in a constant excessive fuel supply to ensure the engine speed is increased while the spark timing is kept constant. As soon as the Starting Phase mode is exited, the control is totally in the hands of the operator, allowing him to proceed as he wishes.

Due to substantial modifications made to the ECU software in this project, certain predefined features, such as Idle Control mode, could no longer be applied directly. The Idle Control was created with the supposition of the engine using a conventional gas mixer, as a venturi-type or a diaphragm. Engines using this type of mixers have different control systems associated. In this way, the Idle Control mode was designed for these control strategies and could not be adapted to the present application. To overcome this limitation, idle control was implemented through a custom ignition timing strategy.

A specific region of the ignition map was created in which the spark timing was deliberately delayed to reduce combustion efficiency. This reduction in efficiency enabled the engine to settle into a stable idle state. More precisely, at around 1000 rpm and with valve openings below 20%, the spark was retarded enough to cause the engine speed to gradually decrease until stable combustion conditions were achieved. Once idle was established, it could be reliably maintained. Exiting the idle region required a value of valve opening above the 20% benchmark to push the engine speed above 1000 rpm. This transition was characterised by an aggressive variation in the engine behaviour, allowing the engine to become prepared to operate under normal operating conditions, out of Idle Control.

The Speed Control mode, on the other hand, remained fully compatible with the new software architecture and was straightforward to configure. Activated via a dedicated software toggle, it allowed the user to set the desired engine speed via a CAN bus signal. Having the demanded speed configured, the control loop is responsible for adjusting the amount of fuel injected to match the actual speed value with the demand value.

In addition to the standard control modes, a second version of the system was developed that allowed torque-based control via CAN bus signals. Furthermore, the system was enhanced to accept throttle commands via the CAN bus, replacing the traditional analogue throttle pedal signal, but also demanded speed commands, ending the necessity to do it directly on the Trijekt software.

Chapter 5

Test Methodology

This chapter outlines the test methodology employed in the testing procedures and data acquisition process, and the process of preparing the complete setup for the final and most complex tests. The content is structured into four main sections to ensure a comprehensive understanding of the setup and its functionality.

First, the simulation tests conducted are described in detail, explaining their preparation and importance. In particular, the ECU logic was validated using hardware-in-the-loop (HiL) methods, without requiring engine operation.

Afterwards, the characterisation of the proportional valve is addressed as a way of verifying the validity of the assumption made during the design process.

Additionally, a detailed description of the test setup is presented, highlighting the key components involved and the data visualised during engine operation, while the measurement systems are explained.

Finally, the test procedures are presented, and all the important details are shown. The present study employs the load-cut protocol. The load-cut tests allow for the analysis of ignition stability, cyclic variability, and combustion phasing in dynamic conditions. The selection of test points was designed to integrate the most realistic operating scenarios pertinent to engine operation.

5.1 Simulation Tests

In the event of the ECU being fully configured, the subsequent critical phase involves the execution of simulation tests before the physical connection of the system to the engine. These simulations are of crucial importance as a validation step, the purpose of which is to assess the ECU's response under various engine operating conditions, as well as to verify the effectiveness of prior software modifications in a controlled environment.

In order to simulate engine speed, a microcontroller-based setup was employed, using an Arduino unit programmed to generate a variable frequency signal. The Arduino is coupled with two rotary potentiometers and a screen display, as shown in Figure 5.1.

Figure 5.1: Engine speed simulator.

One of the potentiometers is dedicated to selecting among the pre-programmed codes stored in the microcontroller, each corresponding to a specific engine configuration. The second potentiometer provides a means of adjusting the simulated engine speed, thereby enabling controlled variation of the test conditions. The display serves a complementary function by offering a visual representation of the generated signal. This facilitates direct comparison between the signal delivered to the engine and the one acquired by the ECU, ensuring both accurate validation and easier interpretation of the system's behaviour. The system is powered through a regulated power supply, and the output signal is directed to the ECU's designated crankshaft position sensor input pins, thereby effectively emulating the engine's rotational behaviour.

An old turntable was repurposed to support CAN bus communication, and a C++ programme was developed to interface with the ECU (Figure 5.2).

Figure 5.2: Engine control turntable.

As can be seen, engine speed demand, engine load demand and ignition angle could be controlled using the switches and sliders existing in the turntable. This was implemented in accordance with the ECU's specific CAN bus protocol to ensure reliable data exchange and full compatibility with the communication architecture.

In order to simulate the gas supply pressure sensor, a variable voltage power supply is directly connected to the corresponding ECU input. This configuration facilitates precise emulation of sensor readings across a defined operating range. Furthermore, a proportional solenoid valve was integrated into the system and connected to one of the ECU's output channels. This facilitated the validation of the ECU's capacity to generate precise control signals and to operate actuators based on the simulated conditions.

The ECU was subjected to a systematic variation in the input signals, thereby ensuring the comprehensive testing of all pertinent operating modes, transitional behaviours, and parameters dependent on control under a broad spectrum of emulated conditions. After the simulation tests, which were deemed to provide sufficient confidence in the ECU's performance and safety, the unit was transferred to the test bench and physically connected to the engine. This phase thus initiated the preliminary calibration process, wherein empirical measurements were utilised to optimise critical control strategies, including fuel delivery and ignition timing, under authentic operating conditions.

5.2 Proportional Valve Characterisation

In order to ensure the accurate configuration of both the valve opening angle and the corresponding fuel demand during engine operation, a comprehensive valve characterisation was carried out prior to implementation. This process also served to validate key assumptions made during the design phase. A two-step experimental procedure was employed in order to achieve the aforementioned objectives. The initial stage concentrated on evaluating the linearity of the flow behaviour concerning the valve opening angle, thereby ensuring predictable and controllable fuel delivery across the operational range while validating some of the pre-made assumptions. The second stage established the relationship between the opening angle and the effective flow area of the graphite disk. This, in turn, has a direct influence on the volumetric flow rate and, consequently, the engine's fuel supply. As illustrated in Figure 5.3, the pipe and instrumentation diagram (P&ID) of the setup utilised for the initial stage demonstrates the configuration of flow measurement and control components, which are designed to assess the performance of the valve.

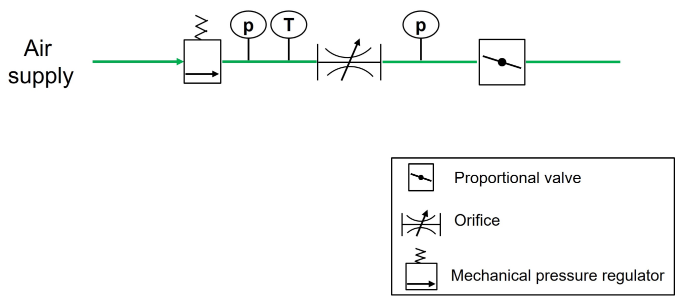

Figure 5.3: First setup diagram.

During the course of the experiment, compressed air was utilised to pressurise the system line, with pressures being measured both upstream and downstream of an orifice plate. Supercritical flow conditions through the orifice were assumed, and confirmed with the pressure measurements, and a discharge coefficient (C_d) of 1 was adopted in order to calculate a theoretical mass flow rate. The flow rate was then calculated for each point recorded, according to pressure and temperature conditions. By measuring the pressure downstream of the valve, and maintaining the same supercritical flow assumption was possible to establish a direct correlation between the calculated mass flow rate, the downstream pressure, and the effective valve opening area.

As illustrated in Figure 5.4, the results for each orifice tested consistently demonstrated a linear relationship between the valve opening angle and the calculated mass flow.

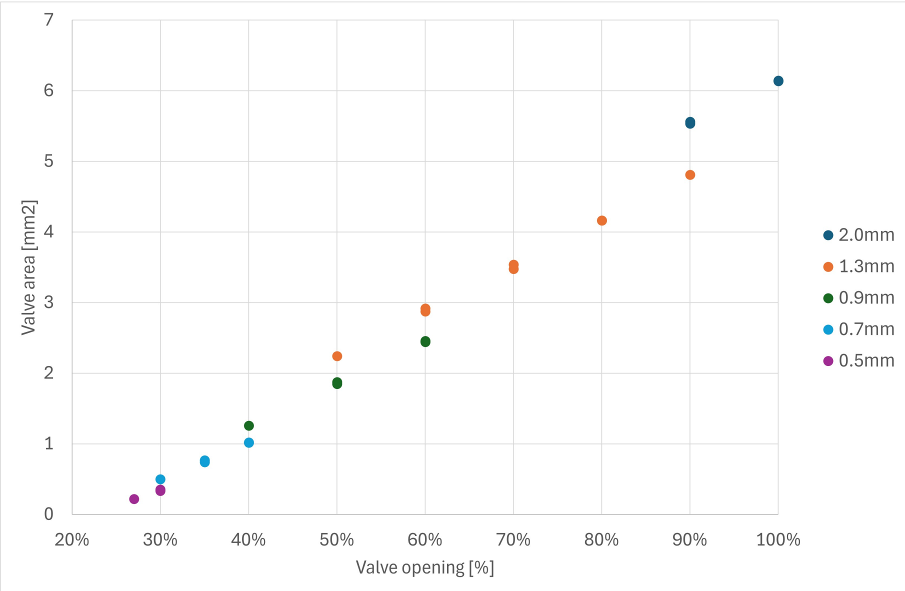

Figure 5.4: Vlave characterisation for several orifices.

This validated the expected flow behaviour under supercritical conditions. While the absolute values of mass flow varied between orifices at the same valve position, this was not a concern at this stage of testing. These discrepancies arose from the assumption of a C_d equal to 1 for all orifices, which is an assumption known to be inaccurate, given that the actual C_d varies according to geometry and flow conditions. The primary objective of this test, however, was not to obtain exact mass flow values, but rather to verify the existence of a predictable, linear flow response to changes in valve position. The precise calibration of mass flow would be carried out later using a more accurate method once the valve had been integrated into the complete fuel supply system.

In order to evaluate the presence of hysteresis in the valve mechanism, the second round of tests was performed in two phases. Initially, the valve opening angle was decreased gradually to the minimum value at which the flow was still supercritical, identified by the pressure ratio upstream and downstream the orifice. Thereafter, the valve was gradually opened until it returned to its original position. The efficacy of this procedure was demonstrated by its ability to identify discrepancies between opening and closing characteristics. As can be seen in Figure 5.5, there is no significant difference between the points measured in both situations.

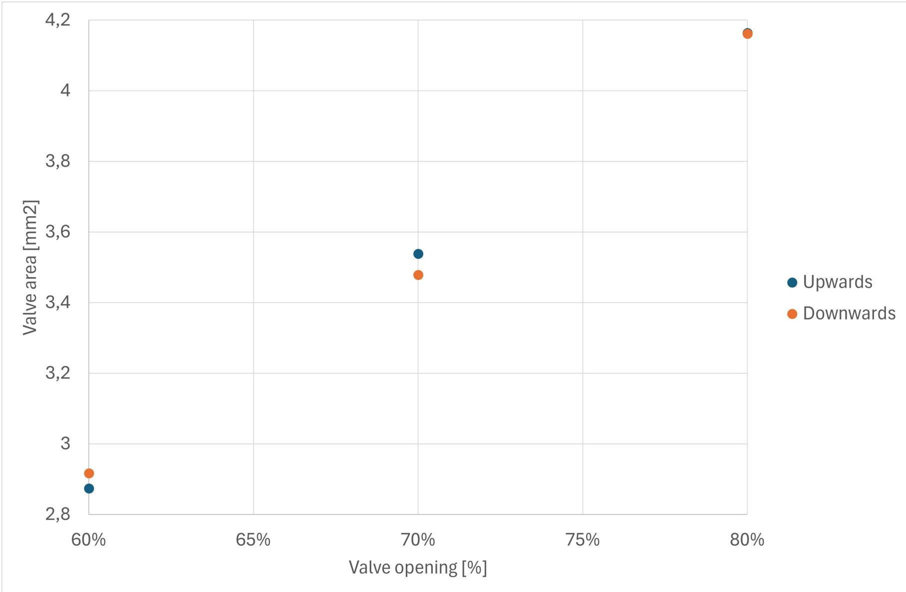

Figure 5.5: Hysteresis verification results.

A 3% deviation was set as a target for this test, and as all the values obtained were lower than this benchmark, the hysterisis was considered despicable and no further adjustments were needed to make to the valve.

The objective of these tests was to verify that the calculated effective area varied linearly with the valve opening angle. This assumption was confirmed under supercritical flow conditions, which were meticulously maintained throughout the experiment to ensure the accuracy and predictability of flow behaviour. Furthermore, a distinct experiment was conducted to investigate the correlation between the calculated area and the valve opening angle under subcritical (undercritical) flow conditions. This test campaign served also as a way of validating the theoretical information regarding flows through orifices described in Section 3.1, especially in Figure 3.1. The results of this analysis, which highlight the deviation from linearity in these conditions, are presented in Figure 5.6.

As previously discussed, the area calculation exhibited a nonlinear behaviour, revealing that the mass flow rate is influenced not only by the upstream pressure conditions but also by the maintenance of supercritical flow across the valve. The results indicate that, as the valve opening increases and the pressure ratio approaches unity, the variation in mass flow rate becomes progressively smaller. This trend aligns with the theoretical expectation that, for undercritical conditions, the flow rate becomes increasingly sensitive to downstream pressure, making it no longer solely dependent on the upstream conditions. These findings underscore the importance of ensuring supercritical flow to maintain a predictable and stable relationship between valve position and mass flow rate.

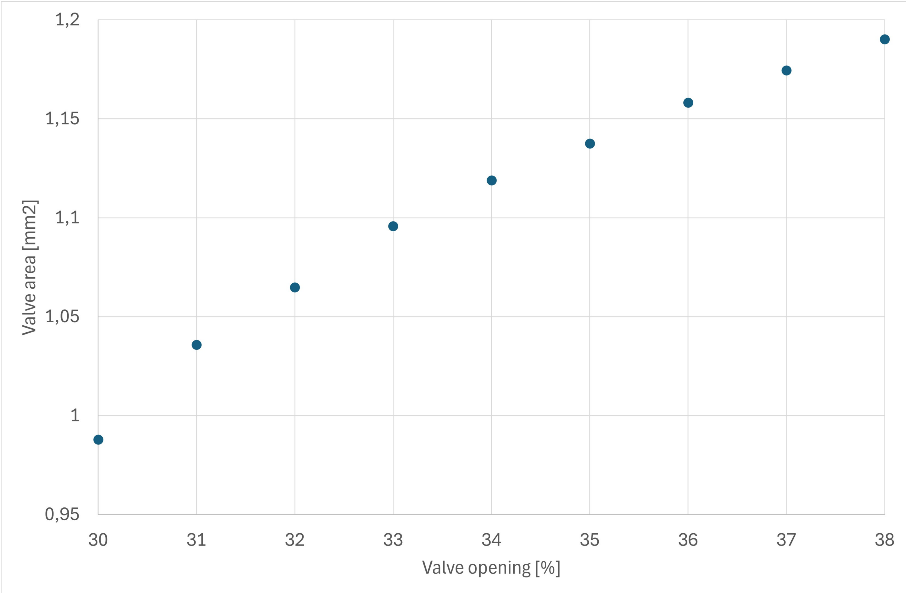

Figure 5.6: Valve characterisation for undercritical flow.

The second stage of the testing process was conducted on the engine test bench, making use of the existing fuel supply line there. This time, the test was conducted under more precise and controlled conditions. The experimental arrangement is illustrated in Figure 5.7.

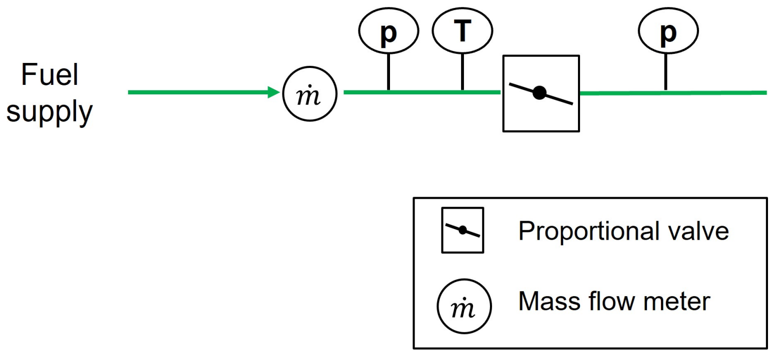

Figure 5.7: Second setup diagram.

In this configuration, the fuel supply line was initially connected to a mass flow meter, followed by its connection to the proportional valve. By measuring the mass flow rate directly in this configuration, it was possible to calculate the effective valve area with greater precision, thereby enhancing the accuracy of engine calibration and control strategies.

Utilising the identical calculation approach as in the preceding step, but now with the measured mass flow rate, the effective area of the valve was ascertained. The testing procedure also included hysteresis evaluation, which was conducted by gradually opening the valve to its maximum position and then closing it in the same controlled manner. Being the procedure similar to the one before, the data was again analysed with the same means. The resulting data, which provide insights into the valve's repeatability and consistency, are presented in Figure 5.8.

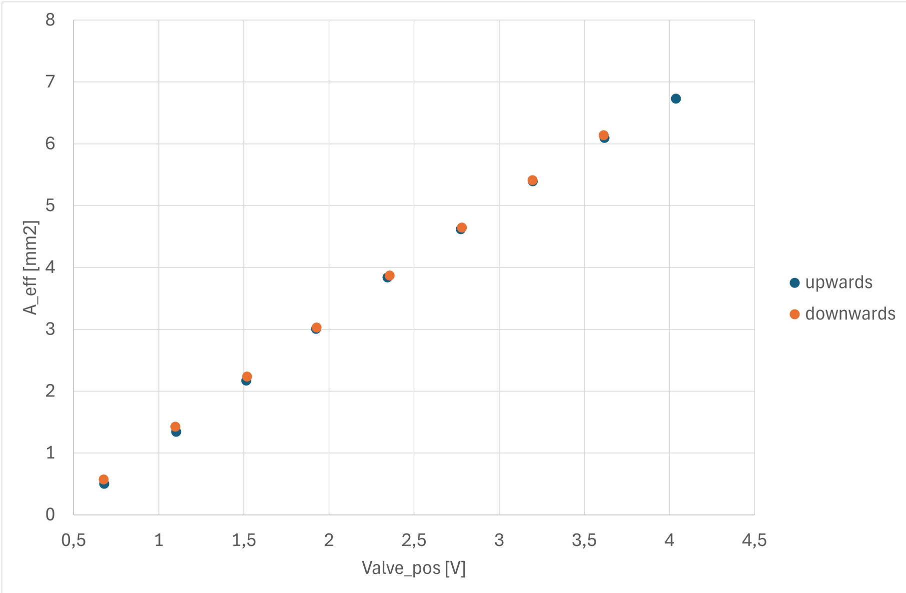

Figure 5.8: Final characterisation of the valve.

As part of the testing procedure, a hysteresis analysis was conducted once more, and no issues were identified. The findings of the present study demonstrated a consistent linear relationship with the results of the preceding evaluation. For the maximum opening angle that was tested, the calculated effective area was 6,70 mm^2. This result was consistent with the earlier valve characterisation that was carried out using the previous graphite disk. This prior characterisation had yielded a C_d of 0,80 for the graphite disk, thus confirming the reliability and repeatability of the valve's performance.

The precise characterisation of the valves thus facilitated the initiation of engine testing and the optimisation of engine control strategies. The findings from the final test were integrated into the ECU and implemented within its control algorithm to ensure precise and reliable fuel delivery during operation.

5.3 Test Stand

The test stand, illustrated in Figure 5.9, functions as the primary platform for the evaluation of the engine's performance under controlled and repeatable conditions. It is a modular setup built inside a container for easier mounting and dismounting, while containing all the necessary components to connect all the required hardware for each different engine. A pivotal component of this configuration is the eddy current brake, which facilitates precise control over engine speed and provides accurate measurement of torque output. This enables not only the indirect calculation of engine power under varying load conditions but also the friction losses in the system. These values can then be compared to theoretical values for the purpose of validation and for benchmarking.

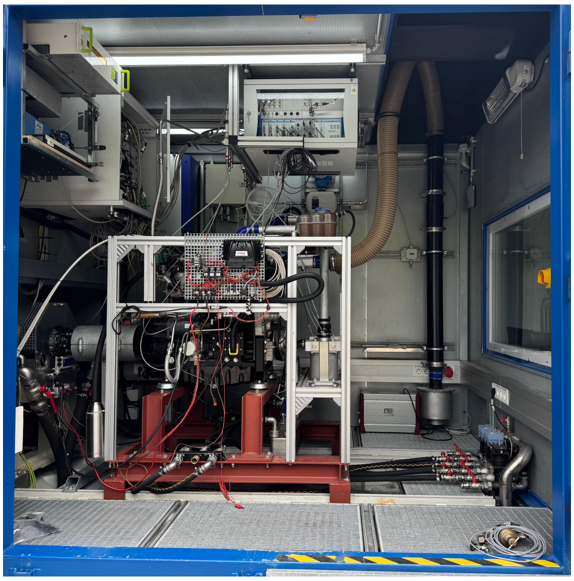

Figure 5.9: Engine mounted on test stand.

As outlined in Section 3.1, the fuel supply system facilitates two configurations: fuel delivery can be facilitated either via the gas mixing unit, situated outside the test container, or through direct connection to pressurised gas cylinders supplied by the fuel supplier, which are also located externally. This flexibility enables safe and efficient testing with different fuel compositions, including syngas mixtures with varying hydrogen content.

The thermal management of both the engine and the eddy current brake is facilitated by a dry cooler that has been installed in close proximity to the container. The operation of the cooler is remotely controlled from the operation room. To facilitate real-time monitoring and data acquisition, the test stand is integrated with an advanced instrumentation system, which displays key performance parameters on dedicated screens located in the operation room (Figure 5.10).

Figure 5.10: Test stand monitoring room

These screens allow operators to analyse engine behaviour and fluctuations over time, ensuring system stability throughout the testing process, but also to control external conditions to the engine as the cooling and the fuel supply.

The two screens on the left provide a comprehensive overview of critical engine parameters, including:

- Engine Rotation speed;
- Engine Torque Calculation and Measurement;
- Cylinder Indicated Mean Pressure;
- Pressure and Temperature at Key Points;
- Air and Fuel mass flow rate;
- Air-Fuel ratio;
- NO_x Emissions;
- Compressor and Turbine Functioning Diagrams;
- Detection of knocking and backfiring.

Each screen is connected to an independent computer, which is responsible for storing the data acquired during all the tests. From the operation room is also possible to control and define the test method, which normally is load-cut, speed-cut or lambda sweep. In load-cut mode, the engine runs at constant speed while the amount of fuel supplied results in a load variation. On the other hand, in speed-cut mode, the engine operates under continuous load, and variations in the supplied fuel result in a corresponding speed variation. For the lambda sweep test, the amount of energy supplied to the engine remains constant while the throttle position is adjusted to vary the air-fuel ratio or lambda, affecting combustion and therefore engine stability.

It is crucial to describe that when testing an ICE, parameters of different natures need to be monitored, which necessitates the use of specialised measurement systems. These systems can be divided into two main groups: indicated data measurements and time-based data measurements.

The first group, indicated data measurements, refers to values that are assigned to specific engine positions, making them cyclical. These values are plotted as a function of the crankshaft angle, with their frequency of acquisition varying with engine speed. In this case, data points are collected 10 times per degree of crankshaft angle. For a 4-stroke engine, each cycle consists of 7200 data points. These measurements primarily include cylinder pressures, which are used to calculate key performance indicators such as IMEP and 50%MFB.

The second group of measurements is based on time-dependent data, which are acquired at a constant frequency of 60 Hz, regardless of the engine speed. These values are not linked to specific engine positions. Time-based measurements include the pressure and temperature at various locations within the engine, such as the inlet and exhaust manifolds and both upstream and downstream of the turbocompressor. Additional readings are taken from the cooling system to monitor pressures and temperatures throughout its components. Still in this group, a portable gas analyser unit from MRU is used in the test stand to evaluate the fuel mixture being transferred to the engine. Therefore, enabling the calculation of the equivalent mass of hydrogen injected and the internal thermal efficiency.

5.4 Test Procedure

In this study, steady-state tests were conducted under controlled thermal boundary conditions. For these tests, the setup shown in Figure 5.11 was mounted.

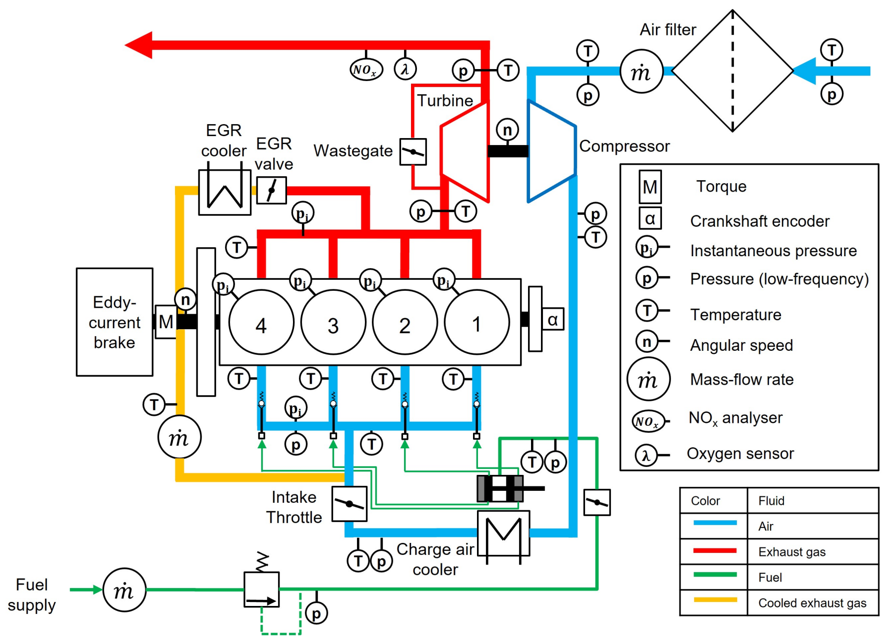

Figure 5.11: Experimental setup diagram.

The coolant temperature was maintained at 90°C at the engine outlet through the utilisation of a closed-loop control system, while the charge air temperature was stabilised at 45°C at the outlet of the charge air cooler. To reduce the influence of short-term noise and transient effects, low-frequency engine and test bench signals, including pressures, temperatures and flow rates, were sampled at 5 Hz and averaged over a 15-second measurement period. To obtain data related to combustion, a set of measurements was recorded in synchrony with the crank angle during 100 consecutive engine cycles. The utilisation of a high-resolution encoder facilitated the acquisition of data with a resolution of 0,1 degrees crank angle (dCA).

The experimental tests were focused on an engine speed of 1500 revolutions per minute (rpm), the same speed the engine is expected to operate on the cogeneration powerplant, and an indicated mean effective pressure (IMEP) range from 2 to 18 bar. Additional tests were performed under constant speed to evaluate the behaviour of the control system. Additionally, tests to evaluate the engine's responsive behaviour during transient load stages were performed. This methodology enabled a comprehensive evaluation of combustion behaviour, efficiency, and engine responsiveness across the expected operation points. Several fuel compositions were tested; the project aimed to focus on a specific composition presented in Appendix B, but others were tested as a way to compare the engine performance under generic commercially available fuels to the ones produced by different engine manufacturers. These compositions are presented in Section 6.4, Table 6.1. For each fuel, engine maps were adjusted, allowing us to have an ECU calibration ready for each of them and allowing us to switch the operation for different fuels in a matter of minutes.

Chapter 6

Results and Discussion

In this chapter, the results obtained from the experimental tests are systematically presented, with emphasis placed on the most significant and technically relevant parameters. Particular attention is given to key performance indicators, such as efficiency, combustion stability, and exhaust emissions, in order to provide a clear and comprehensive overview of the engine's behaviour across the different operating conditions investigated.

Subsequently, the findings are critically examined and compared with theoretical expectations and design assumptions. This discussion not only highlights areas of agreement and deviation but also seeks to elucidate the underlying causes of observed trends. In doing so, the analysis bridges the gap between the idealised system design and its real-world performance, thereby offering deeper insights into both the effectiveness of the implemented control strategies and the limitations imposed by the physical configuration of the hardware.

6.1 First Load-cuts

Following the completion of the preparatory procedures for the engine's operation, the initial load-cut procedures were conducted. For the purpose of these tests, two distinct fuel compositions were selected. The initial mixture comprised 95% H_2 and 5% CO_2. In the second mixture, the CO_2 content was augmented to approximately 10%, with the remaining composition consisting of H_2. The concept of the mixture was to gradually introduce CO_2 to enhance the fuel flow demanded by the engine. In the course of these experiments, the behaviour of both the fuel supply system and the ECU software could be evaluated.

As illustrated in Figure 6.1a, the equivalent mass of H_2 increases in proportion to the rise in engine load (IMEP). Figure 6.1b presents the fuel mass flow rate, measured in milligrams per combustion cycle, which is injected into the cylinder during each combustion cycle. As anticipated, an increase in the mass of fuel injected is directly proportional to an increase in the work produced by the engine, and the value is proportional to the fuel's LHV. About the point at which the combustion of half the fuel mass occurs, Figure 6.1c demonstrates a relatively variable operation, oscillating between 6 and 14 dCA ATDC. In experimental trials, several authors identified that the maximum efficiency of the engine is attained when the 50%MFB point is situated between 8 and 10 dCA ATDC. Consequently, it can be posited that the combustion process was not optimised during the present test. This can be attributed to the fact that there was a paucity of interest in the engine parameters, given that the primary focus of the initial test was on the evaluation of the software and hardware modifications.

Concerning the initiation and duration of combustion (see Figures 6.1d and 6.1e), these mixtures do not demonstrate a particularly distinct behaviour. The mixture with a higher H_2 content demonstrates slightly accelerated initiation of combustion at specific points, while the combustion duration remains constant for both mixtures.

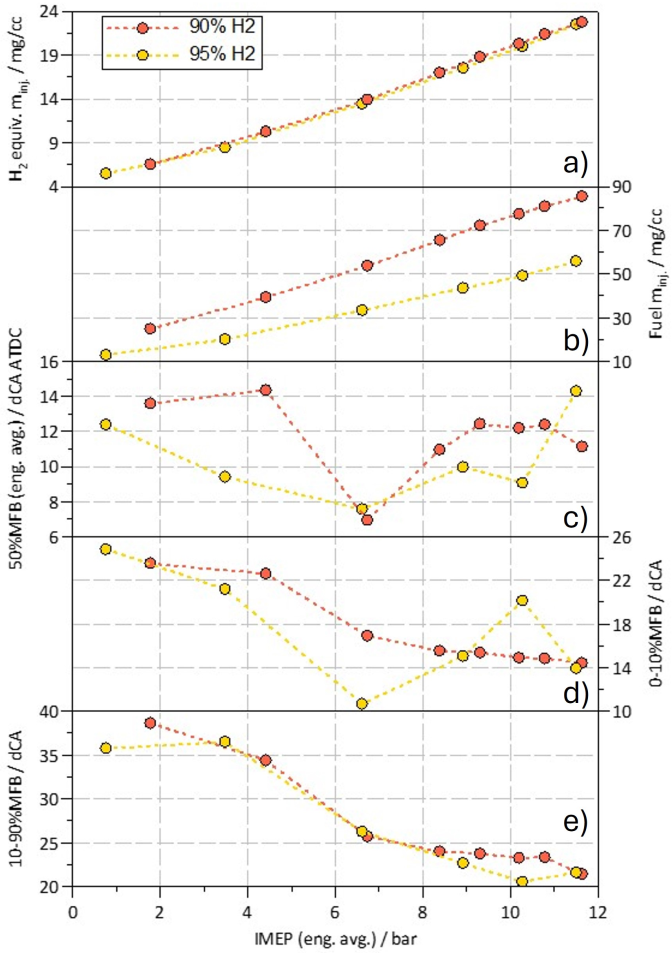

Figure 6.1: First tests combustion parameters.

An important operational parameter is the coefficient of variation (CoV), which is generally considered acceptable below 3%. As Figure 6.2a shows, most of the operational points in these tests fulfilled this requirement, with the exception of those corresponding to lower loads, which are not very relevant to this study. The exhaust gas temperatures entering the turbine were not excessive, reaching a maximum temperature below 500°C (Figure 6.2b), not resulting in any damage to the hardware. As expected, the air-fuel ratio (λ) decreased with the amount of fuel injected, since no throttling was applied to the engine in this test phase. However, a minimum value of 2,0 was established to maintain stable engine behaviour (Figure 6.2c). Internal thermal efficiency (ITE) varied from an inefficient 10% to 39%, and behaviour was similar for both fuels, as can be seen in Figure 6.2d. Regarding emissions, the values were negligible across the entire testing range, as the maximum value was less than 0,2 g/kWh, five times lower than the target set for these tests in this laboratory (Figure 6.2e).

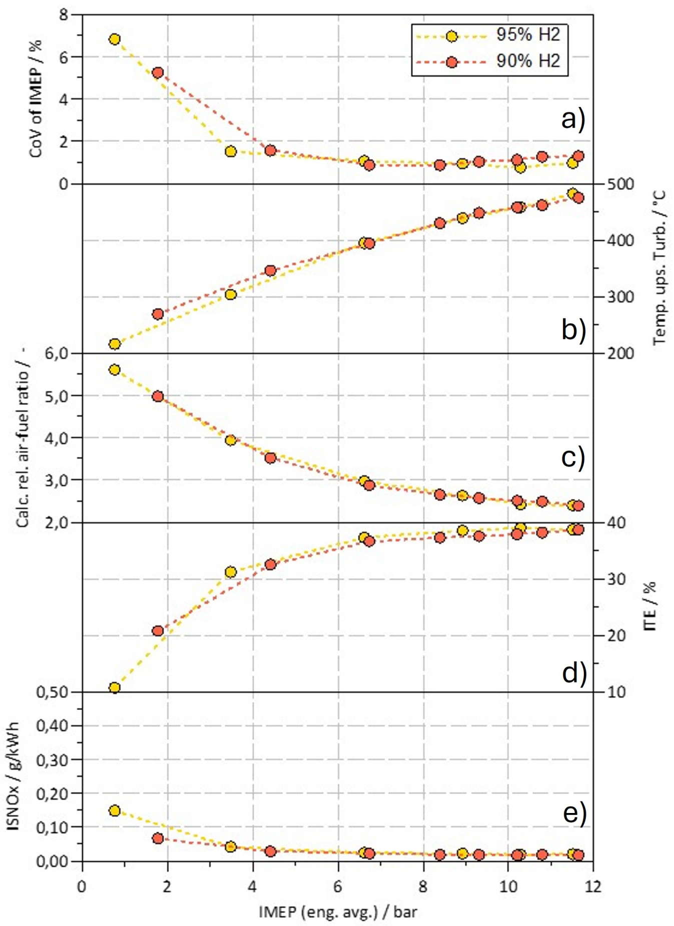

Figure 6.2: First tests engine output.

During the first series of tests, it was found that the behaviour of the fuel injection was not what one expected. Actually, for the measured conditions, the pressure values measured at the fuel injection outlet and the supply were too close, demonstrating the capability of the supply system being short. This meant that the line had excessive flow restriction and would likely be unable to deliver the expected amount of fuel. To better understand this, some small modifications were made to the engine, which are described in Section 6.2.

6.2 Testing After Adjustments

As described earlier, the behaviour of the fuel supply system during testing did not meet the initial expectations, showing performance limitations that hindered the intended operating flexibility. In this context, it became necessary to consider possible modifications aimed at improving the system's behaviour. The overall strategy for these modifications was guided by the principle of implementing the simplest and least invasive changes first, thereby allowing a stepwise optimisation while minimising the risk of introducing new uncertainties.

The initial focus was placed on identifying components in the supply line that could be responsible for unnecessary pressure losses or flow restrictions. One such candidate was the set of injection lance tips, illustrated in Figure 6.3. These tips presented two potential drawbacks: on the one hand, their internal geometry could contribute to a reduction in effective flow area, and on the other hand, each tip incorporated a check valve. Although the check valves were originally installed to prevent backfire during the early stages of engine development, subsequent testing demonstrated that this risk was negligible under the present configuration. As a result, their function was no longer essential, and their presence became a potential source of unwanted restriction.

Consequently, the decision was made to remove the lance tips altogether and reconfigure the injection system without them. This modification was expected to reduce flow resistance, stabilise the pressure distribution, and ultimately enhance the predictability of the mass flow supplied to the engine. The removal also simplified the architecture of the supply line, thereby facilitating diagnostics and reducing the number of potential failure points. In addition, the absence of check valves eliminated possible dynamic effects, such as valve lag or partial blockage, which could have negatively influenced transient response during load variations.

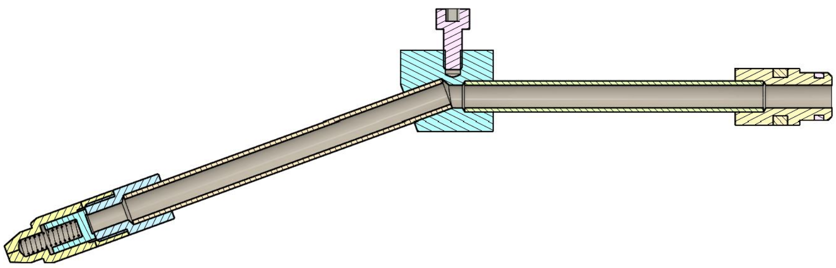

Figure 6.3: Injection lances.

Additionally, a pressure sensor was connected to the distributor, giving additional information regarding the fuel state in the distributor chamber to help identify the choking point of the system. Having the lances removed, all the rest of the setup was mounted again, and the tests were continued.

This time, the last composition featuring 90% was tested to establish a comparison between the system with and without the lances. Afterwards, a fuel composition featuring 85% H_2 content, completed with CO_2, was used due to its lower LHV when compared to the previous one.

According to the design calculations and experimental tests with similar systems, the pressure ratio between upstream and downstream of both the proportional valve and the distributor should remain below the value of 0,55. In this sense, and remembering that the fuel supply pressure remained between the values of 10 and 11 bar throughout the tests, the maximum allowable pressure downstream the valve should be below 6 bar.

Figure 6.4 suggests that for IMEP values higher than 6,1 bar, the distributor is unable to maintain the expected behaviour of supercritical flow. This limitation creates excessive upstream pressure and does not allow for an efficient and controlled fuel delivery. The limitation is even more evident for IMEP values of 12 and 14,3 bar, situations in which the pressure upstream of the distributor is almost the same as the supply pressure, demonstrating a massive choke in this area. Additionally, the fluctuating nature of the pressure value throughout the whole test was something that was not expected and could indicate that other problems were arising in the supply line.

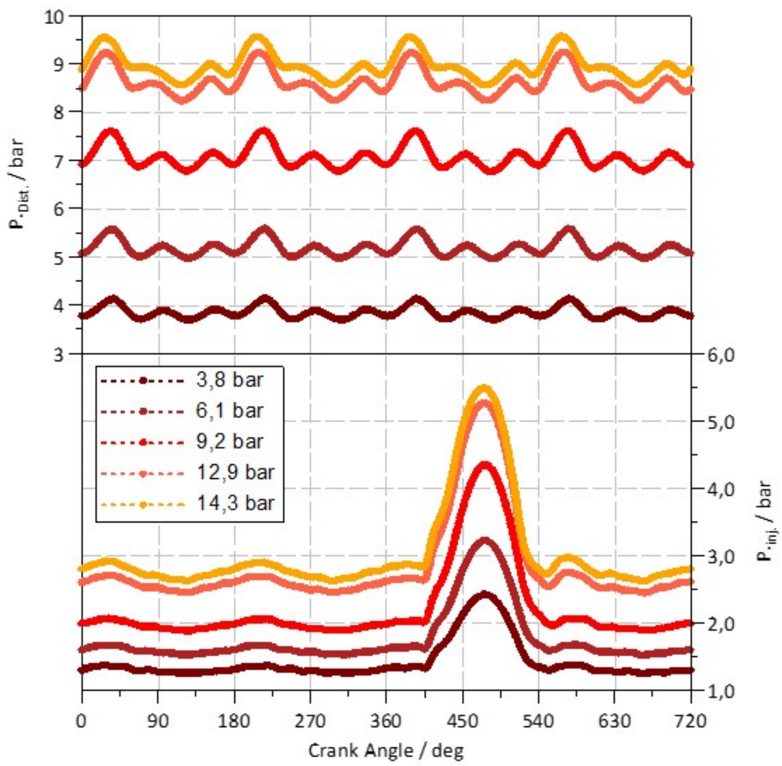

Figure 6.4: Distributor and injection pressures over dCA.

As can be seen in Figure 6.5, combustion properties were pretty similar to what had been seen in previous testing. As expected, the equivalent mass of H_2 increases in line with the increase of IMEP (Figure 6.5a). The linear behaviour proves that the efficiency suffers only small variations through the test range spectrum. This time, it was possible to test the engine from 9 up to 26 mg of H_2 equivalent per combustion cycle.

Naturally, the fuel mass flow was higher for the mixture containing 85% H_2 content due to its lower LHV (Figure 6.5b). In this test, the ratio of CO_2 slightly dropped for the higher loads due to low pressure on the supply bottle, as can be identified when evaluating the mass of fuel injected. For the 85% H_2 mixture the maximum fuel possible was achieved at around 110 mg/cc of fuel as the valve was already opened at its maximum.

This time, the combustion was optimised, and with this, the 50%MFB point could be targeted to about 10 dCA at each point (Figure 6.5c). Some small variation across the tests were obtained for the 50%MFB but they are not relevant as they never surpassed the values of more than 1 or 2 dCA. Even with the small variations, the values were well within the range of optimal combustion for both cases. The beginning of combustion and its duration (Figures 6.5d and 6.5e) stayed in line with what was previously observed during the other tests. For both mixtures, they decreased with the increase of IMEP due to earlier spark timing applied, in the first place, but also due to the spread of combustion speed increasing with the pressure inside the amount of fuel inside the cylinder.

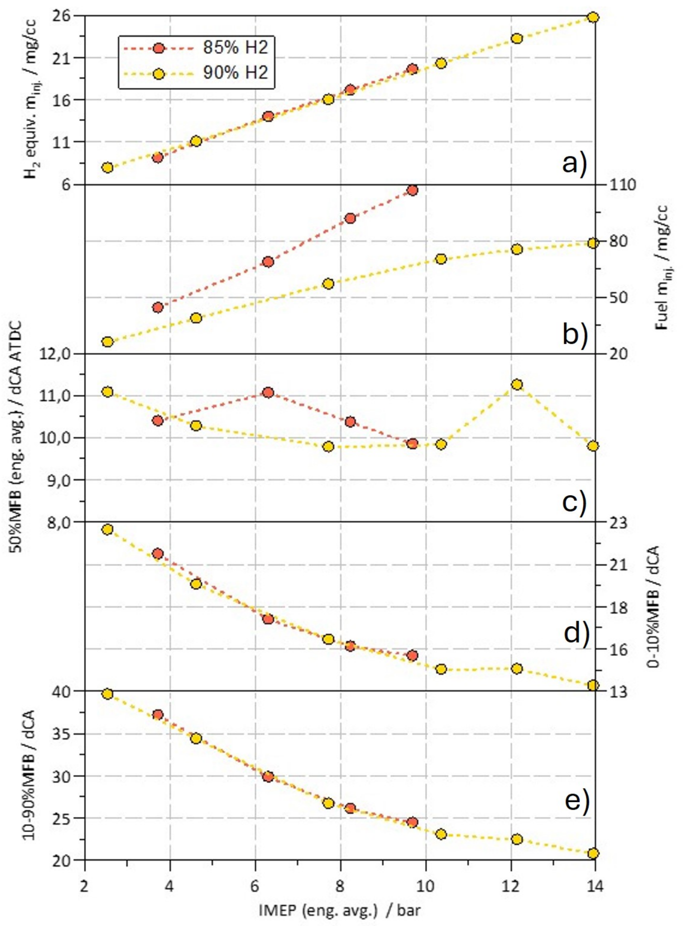

Figure 6.5: Second tests combustion parameters.

Regarding the CoV of combustion, this time all the points presented satisfactory behaviour, keeping this value below the target of 3% (Figure 6.6a). This stable behaviour is a good indicator of the correct air-fuel ratio management. Exhaust gas temperatures entering the turbine presented similar behaviour to before as well (Figure 6.6b), not exceeding 500°C, which is quite satisfactory.

The λ was kept between 4,5 and 2,3 as before since no throttle control was applied to the engine intake (Figure 6.6c). For the thermal efficiency, the values remained pretty similar, only showing a small decrease in the mixture with lower H_2 content (Figure 6.6d). As expected, the tendency is for the compositions with higher hydrogen content to exhibit higher ITE values due to hydrogen's combustion properties. For the emissions, still, no problems arose as the values started well below the target of 1 g/kWh (Figure 6.6e), being negligible during the whole test spectrum.

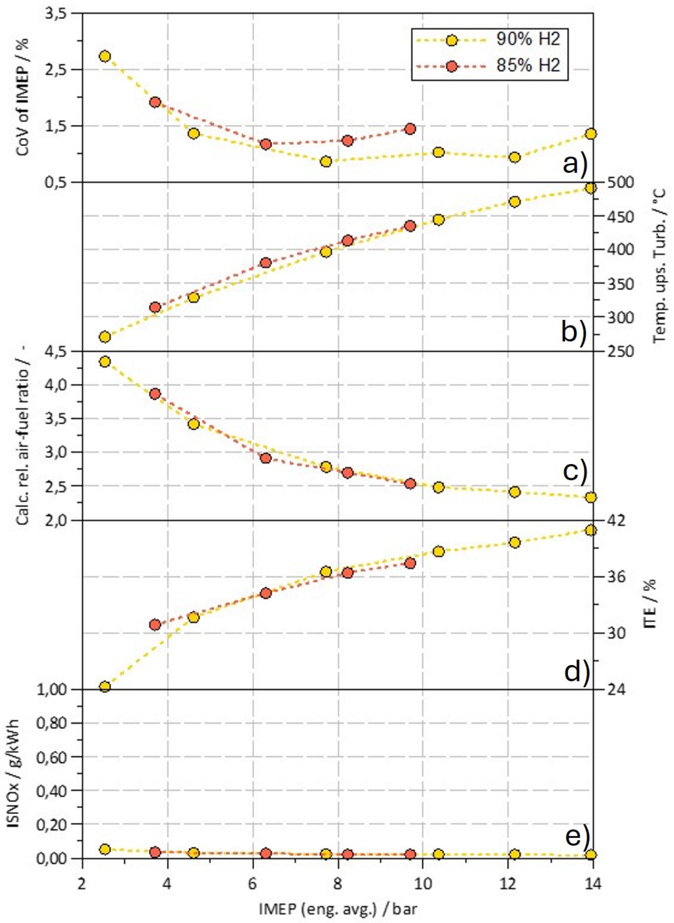

Figure 6.6: Second tests engine output.

With this second campaign of tests, we could understand that the check valves in the lances were not a limitation, as a small difference was noticed after removing them. Additionally, with the pressure sensor in the distributor, we could understand that the low flow was not due to excessive pressure losses in the fuel lines since the choke point could clearly be identified. The limitation to the flow could be found in the geometrical restrictions of the distributor overlapping disk, reflecting the necessity for a design of a new distributor, bigger and prepared for the adequate mass flows needed by the engine.

6.3 Testing with Syngas

Understanding that the supply system would not fully satisfy the engine's fuel requirements as initially expected, it was nevertheless considered valuable to conduct additional testing. The idea was that, even if the ideal operating scenario could not be achieved, systematic testing would still provide meaningful insights by revealing the precise limitations of the system under different operating conditions. This approach also enabled a direct comparison with the performance of the older setup, thereby establishing a benchmark against which improvements or shortcomings could be objectively assessed.

The baseline composition of the syngas used in this project was defined by the Fraunhofer Institute and served as the primary reference. From this base case, a series of alternative fuel mixtures was generated by progressively enriching the hydrogen content while maintaining the relative proportions of the other constituents constant. The exact details of these compositions are presented in Appendix B, ensuring full transparency and reproducibility of the experimental conditions.

The order of testing began with pure hydrogen, followed by mixtures of successively lower LHV. This sequence was deliberately chosen to initiate the characterisation of the system with fuels that posed fewer operational challenges before gradually advancing towards those expected to impose greater demands on the supply and control systems. Such a stepwise approach reduced the risk of premature test interruptions and facilitated a more structured identification of failure modes.

In anticipation of the need for intake throttling, particularly when operating with low-LHV mixtures, an external controller independent of the ECU was integrated into the test bench. This device actuated the throttle body and allowed precise variation of its position, thereby enabling real-time adjustment of the intake air mass. The availability of external throttle control was essential for maintaining stable operation across the different fuels, as it directly influenced the air–fuel ratio — the key parameter governing combustion stability, efficiency, and emissions. By incorporating this additional control element, the testing programme was able to capture a more complete picture of the engine's adaptability to diverse fuel compositions.

As can be seen in Figure 6.7a the throttle remained open for most of the test, only for the 40% H_2 mixture some throttling was needed due to combustion instability, as it is presented later. The valve opening angle is presented in Figure 6.7b. As shown, for pure hydrogen, there was no limitation from the valve, but for the other compositions valve's maximum opening was achieved. This meant that the engine operation was being limited by the amount of fuel supplied by the line, as expected from the previous test findings. Equivalent H_2 mass injection remained directly proportional to the engine load and stable throughout the tests up to a maximum of 31 mg/cc, corresponding to an IMEP of 16 bar (Figure 6.7c). For the three mixtures presenting lower LHV, the maximum value of IMEP obtained was of 14, representing a considerable loss, 12,5%, when compared to the one obtained by pure hydrogen.

Regarding the injected fuel mass per combustion cycle, the mixture with 40% H_2 presented the highest values, providing the reference for maximum flow capacity of the system, about 140 mg/cc, which is more than four times the amount of hydrogen (Figure 6.7d). The 50%MFB was optimised most of the time, being between 9 and 11 dCA ATDC, the exception is for some higher load tests on pure hydrogen (Figure 6.7e). This delay in the combustion phase was created on purpose to avoid harmful emissions. Regarding the beginning of combustion, the behaviour presented a similar tendency across the whole spectrum of fuels, reducing with the increase in engine IMEP (Figure 6.7f), being the lowest value found for pure hydrogen due to its highest flame propagation speed.

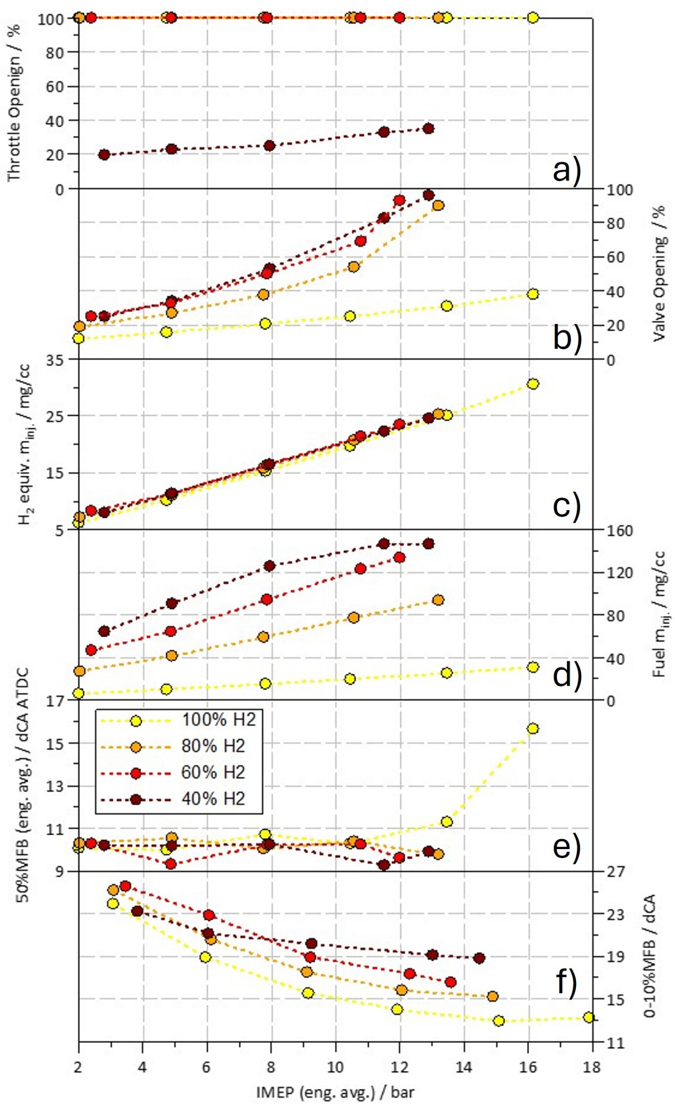

Figure 6.7: Syngas tests combustion parameters.

The duration of combustion, as seen in Figure 6.8a, still presented the tendency to decrease with the increase in IMEP for all the fuels. The lower values were found for pure hydrogen, showing bigger disparity to the other fuels on higher loads. This values stayed in line with what was previously found. Through throttling, as referred to in previous sections, the CoV of the 40% H_2 was controlled to be below 3% across the whole test spectrum (Figure 6.8b). For the other mixtures, the lower load range presented some CoV values up to 6% in some conditions, which were not very relevant. For the operational spectrum, the CoV was quite satisfying across the four mixtures.

For the values of the exhaust gases upstream the turbine, the values were pretty similar across the several mixtures while no throttling was applied (Figure 6.8c). The adjustment of the throttle body position resulted in higher exhaust temperature due to a lower λ (Figure 6.8d). The ITE values were very consistent between the mixtures, only being noticeable a small increase in efficiency with the increase in hydrogen content (Figure 6.8e). Through the whole test, the NO_x emissions stayed constant and at a very low a safe level, being the maximum (0,10 g/kWh) ten times lower than the target established (Figure 6.8f).

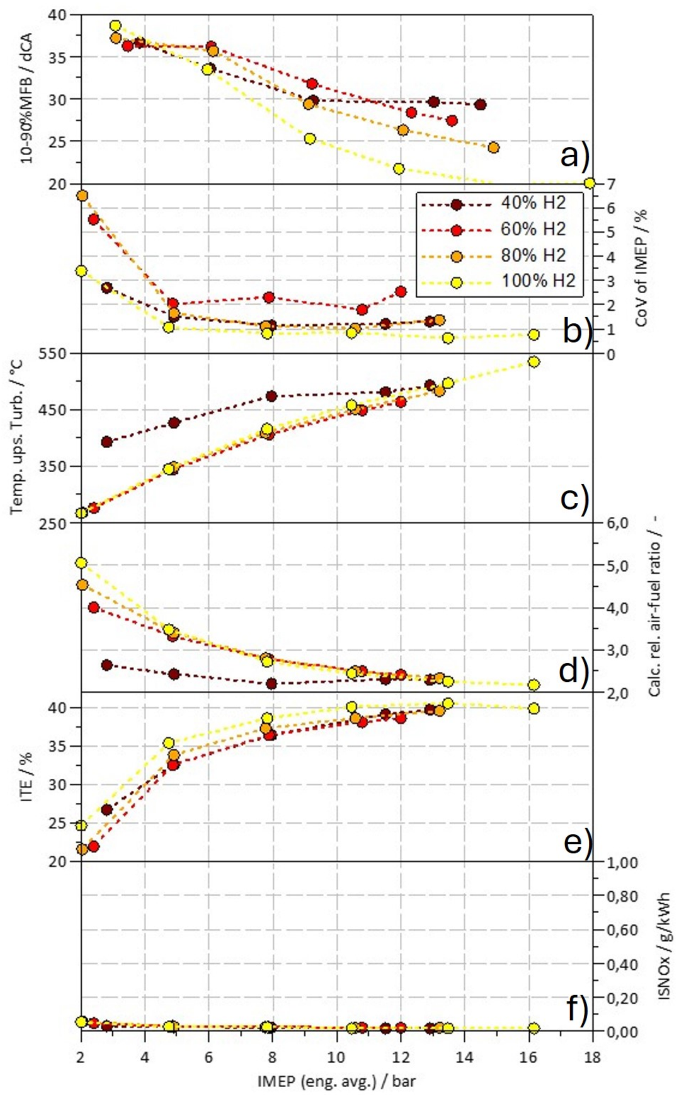

Figure 6.8: Syngas tests engine output.

6.4 Complementary Testing

As demonstrated in the preceding sections, the results obtained for the system did not fully align with the initial expectations. This outcome highlighted the importance of broadening the testing perspective and benchmarking the engine's behaviour against reference practices adopted in the industry. In this context, it became increasingly relevant to evaluate the performance of the adapted engine using fuel compositions similar to those conventionally employed by engine manufacturers when developing engines designed for alternative gaseous fuels.

To this end, a targeted review of technical data from manufacturers specialising in engines for alternative gases was conducted. Based on this information, representative compositions were identified and used to establish a set of benchmark fuels. These compositions, which serve as an industry-oriented comparison framework for the present study, are summarised in Table 6.1.

Table 6.1: Fuel composition and lower heating value [38, 39]

Mixture	CO_2	CH_4	LHV (MJ/kg)
Biomethane	0,0	100,0	50,0
Biogas	35,0	65,0	20,2

The first step in testing was to make a lambda sweep test campaign. In this campaign, the amount of chemical energy supplied to the engine remains constant while the throttle position of the engine is adjusted to vary the air-fuel ratio. This throttle adjustment allows for finding the optimal values of air-fuel ratio for engine operation while evaluating the combustion stability across the range of λ values.

As Figure 6.9a suggests, the throttle opening was progressively increased from a minimum value of 13% up to 17%, which allowed for operating under lambda values between 1,0 and 1,8. Valve opening remained constant during the test, being the value only dependent on the composition of the fuel, 6.9b. Naturally, the opening was greater for the mixture containing CO_2 due to its lower LHV. The amount of chemical energy supplied to the engine was kept constant at an equivalent hydrogen mass of 9 mg/cc, 6.9c. Fuel injection is, naturally, proportional to the valve opening since all other variables are kept constant. This way, it presents the same behaviour as the valve opening, 6.9d.

The timing of 50%MFB was kept constant due to spark timing adjustment, and the values were kept at around 10 dCA as in previous tests, 6.9e. Regarding combustion start, its duration increased, for both fuels, with the increase of air-fuel ratio as a result of the decrease of fuel concentration in the combustion chamber, 6.9f. As expected, the mixture presenting lower LHV presented slower combustion, in some cases being almost 40% higher when compared to the other mixture.

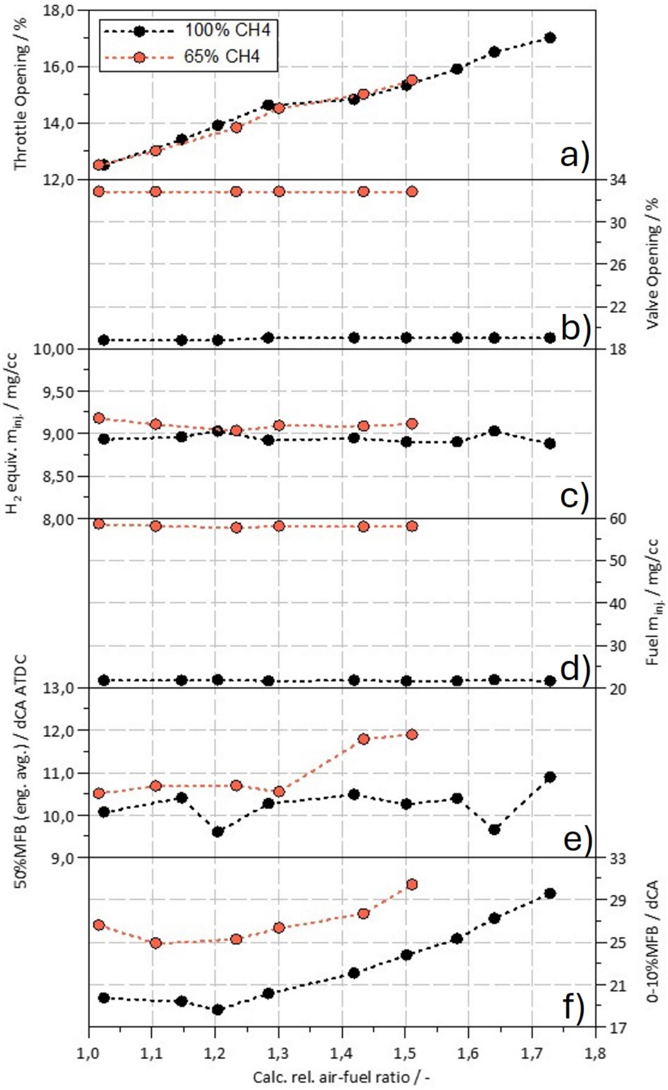

Figure 6.9: Lambda sweep combustion parameters.

The duration of the whole combustion tended to increase with the increase in air-fuel ratio as it becomes more diluted, for both fuels, 6.10a. The CoV of combustion was low in both cases for air-fuel ratios below 1,4, 6.10b. For higher values, it increases exponentially, exceeding the targeted limit of 3%. This analysis allowed us to understand that the limit for stable operation was at an air-fuel ratio of 1,4. The temperature measured at the turbine entry peaked for the lowest air-fuel ratio at a maximum of 610 °C, not presenting harmful values for the engine, 6.10c. Internal thermal efficiency presented a maximum value of 30% for pure methane at lambda 1,4 and a maximum of 27% for the diluted mixture at lambda 1,3, 6.10d. Both fuels ITE presented a negative parabolic behaviour, favouring the operation under a medium value of lambda. As for emissions, the lower air-fuel ratio is directly related to high emissions, up to values of 12 g/kWh, 6.10e. Only for lambda values above 1,4 for 65% CH_4 mixture and 1,5 for pure CH_4, the emissions tended to acceptable values, something already expected due to the unclean nature of methane combustion.

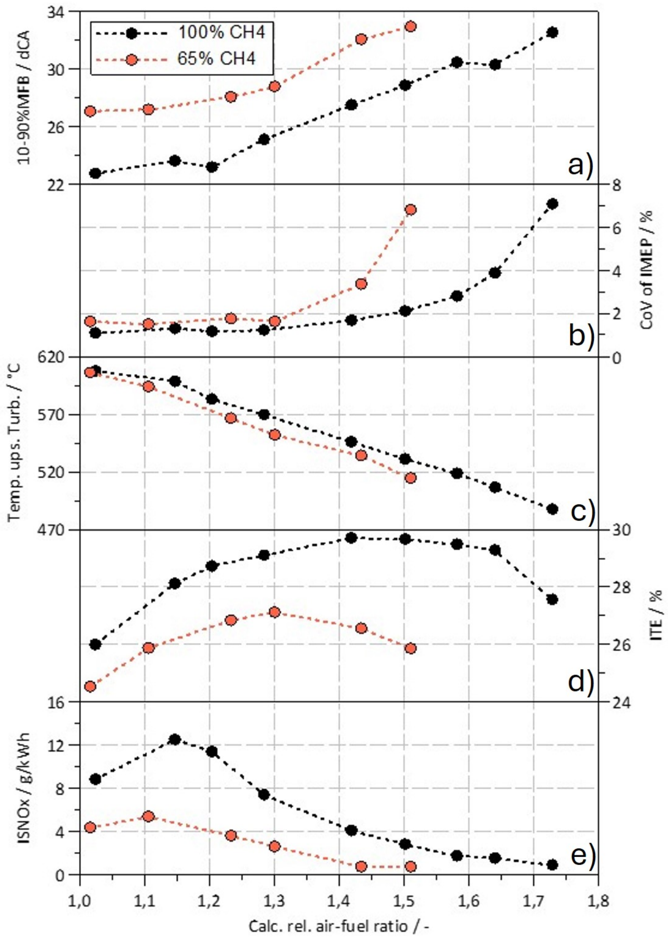

Figure 6.10: Lambda sweep engine output.

Having the lambda sweep tests realised, it could be understood that the most stable and efficient operation point for the engine was to keep the lambda values between 1,4 and 1,5, depending on the mixture. With this characterisation, the load cut test could be performed to evaluate the engine's behaviour under these fuels.

For these tests, in opposition to what happened with pure hydrogen, there was a necessity for engine throttling due to its low combustion stability across a wide range of air-fuel ratios, 6.11a. The valve opening presented an almost linear dependency on the engine's IMEP for pure methane while for the other mixture a different behaviour was found due to its geometric characteristics. Valve's position reached maximum opening for the 65% CH_4 content, while for pure methane it did not present a bottleneck 6.11b. The equivalent amount of H_2 injected presented linear behaviour with the engine IMEP and was accurate between different mixtures 6.11c. Regarding the mass fuel injected, the maximum value measured was about 170 mg/cc, limited by the fuel supply system 6.11d, as described before. For all fuels, the combustion was optimised, occurring the 50%MFB at around 10 dCA ATDC 6.11e. As expected, the lower the LHV, the longer the time for the combustion to take place. For higher loads, the beginning of combustion of the 65% CH_4

mixture took about 20% more time than for pure methane (6.11f). In case of trouble arising at this stage, platinum spark plugs were prepared to be used to mitigate the problem due to their higher reactivity.

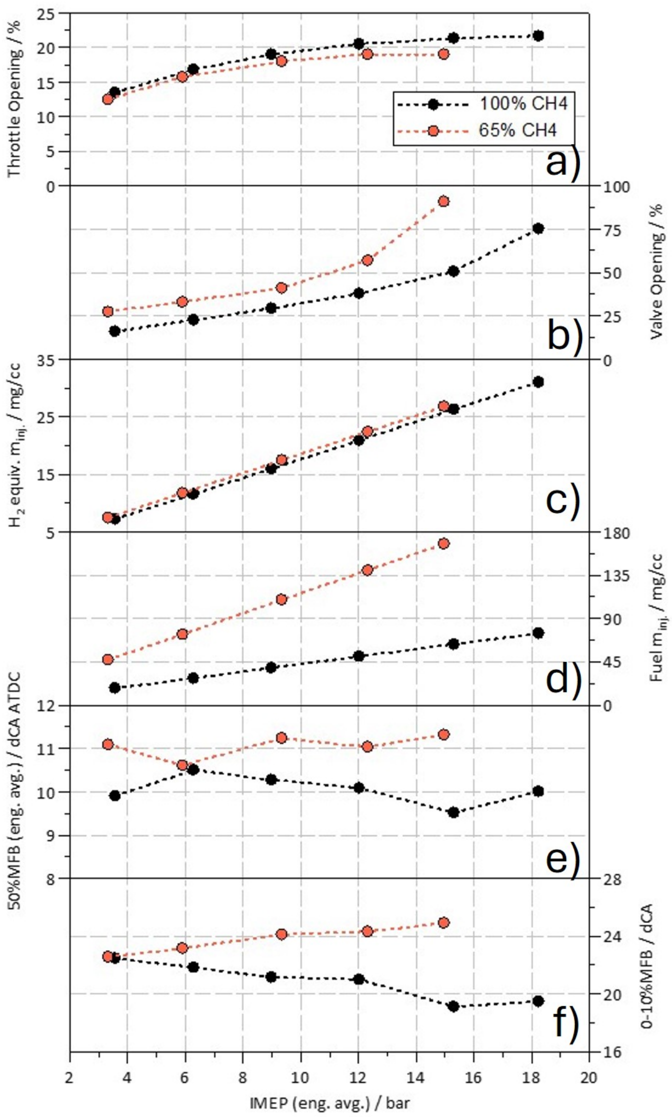

Figure 6.11: Reference fuels combustion parameters.

Regarding the duration of combustion, the values were fairly similar across the several mixtures, with pure methane showing the biggest variation with the load, as shown in 6.12a. The CoV values were kept low across the whole test spectrum due to the use of engine throttling, as expected, 6.12b. Temperatures of the exhaust gases were pretty similar for both mixtures and were not problematic, 6.12c, due to the similar λ, 6.12d. Even though the values went up to 680°C, it was not a problem, and the hardware did not present any defects. Looking at the ITE, the values did not present massive differences across the fuels, but it was clear that pure methane was the most efficient, gaining up to 2% over 65% CH_4 mixture, 6.12e. Lastly, regarding emissions, methane mixtures presented quite high emissions up to 8 and 10 g/kWh of NO_x particles, 6.12f. This is the major drawback associated with this type of fuel for this apllications.

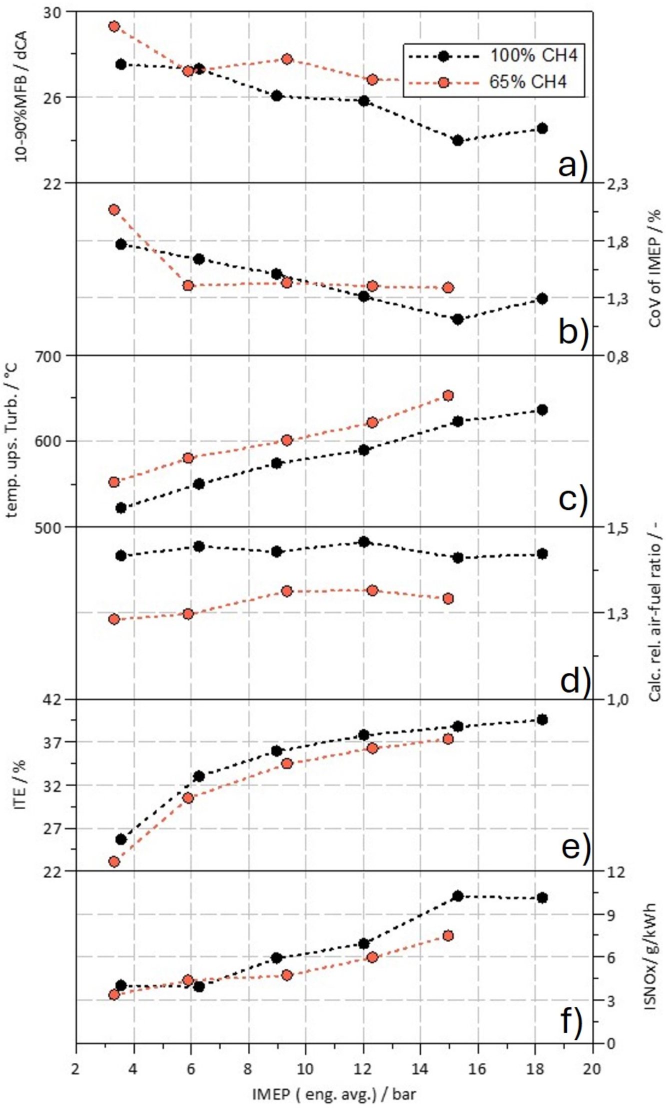

Figure 6.12: Reference fuels engine output.

With the experimental setup in place, it was possible to successfully test the two conventional, commercially available mixtures and also hydrogen without significant operational issues. The only challenge arose for the lower-LHV fuel, which was limited by the supply line. The comparative analysis of these three fuels offers a valuable framework for assessing not only the performance and reliability of the developed system but also the broader prospects of ICE technology operating with alternative fuels. These insights will be further explored and discussed in detail in Section 6.5.

6.5 Discussion

In this study, two main aspects were developed: one related to *software* and the other to *hardware*.

From the software perspective, both the design of the control strategy and its implementation produced highly satisfactory results. The system operated as intended, and most of the difficulties encountered during testing could be resolved through iterative adjustments. Importantly, the adopted architecture proved versatile and robust, posing no obstacles to the overarching objective of enabling engine operation with a wide spectrum of gaseous fuels, regardless of their specific characteristics. In this respect, the software component of the work can be considered fully successful.

The hardware, on the other hand, did not entirely fulfil the intended purpose. While it validated the design assumptions and behaved consistently with expectations, it ultimately lacked the capacity to supply the engine's full fuel demand. For commercially available mixtures, operation was nearly flawless, which is an encouraging outcome. However, the limitations of the system became evident when applied to fuels with low-LHV. When compared to the older version, whose results are presented in Appendix C, the new system did not allow for higher mass flows at this stage. Nonetheless, a key positive aspect is its scalability potential, which was not achievable with any of the previously tested configurations. This distinction highlights the value of the present design, as it provides a pathway for future adaptations and optimisation. Overall, while the hardware proved too constrained in its current scale to guarantee proper operation across the entire range of fuels considered, its architecture lays the groundwork for further developments.

Chapter 7

Conclusions

This chapter provides a comprehensive overview of the project, including a summary of its principal achievements and an examination of the challenges that were encountered. The discussion highlights both the positive and negative aspects of the work, providing a balanced evaluation of the developed system. Furthermore, potential strategies for future improvements are outlined, with particular emphasis on the most promising solution identified during the course of the research.

7.1 General Conclusions

The present study investigated the feasibility of converting a heavy-duty ICE to operate on pyrolysis gas of varying compositions, with particular emphasis on hydrogen enrichment as a means of improving performance and reducing emissions. In order to facilitate such operations, a novel fuel delivery architecture was developed. This architecture is centred on a proportional valve and a custom distributor, and is supported by extensive modifications to the ECU's software. The proportional valve was characterised through experimental means, thereby confirming a linear relationship between opening angle and effective flow area under supercritical conditions. This relationship thus enabled the predictable control of mass flow rate. The ECU was reprogrammed to calculate fuel delivery in real time from valve position, supply pressure, and engine speed. In addition, advanced control strategies were implemented to stabilise idle operation and to allow torque or speed control via CAN bus, ensuring precise adaptability to different fuels.

The experimental testing phase of the project demonstrated that the adapted system could operate reliably on a wide range of gaseous fuels. These ranged from pure hydrogen to hydrogen-enriched syngas and conventional alternatives such as biomethane and biogas. Pure hydrogen operation yielded the highest thermal efficiency, approaching 39%, with extremely low NO_x emissions, well below the laboratory target, and stable combustion without the need for throttling.

Furthermore, hydrogen-enriched syngas demonstrated favourable combustion stability and efficiency, confirming that the implemented ECU updates and control strategies functioned exactly as intended. At lower hydrogen fractions, however, the increased mass flow demand exposed the geometric limitations of the distributor, revealing that the main bottleneck was not the control logic but rather the physical size of the fuel delivery components. Conventional methane-rich fuels achieved efficiencies comparable to hydrogen, but produced substantially higher NO_x emissions, in some cases up to 10 g/kWh. This is difficult to mitigate due to their operating limitation at air–fuel ratios near 1.4–1.5.

When compared with the previous setup (Appendix C), the results indicated that, in terms of hardware performance, the limitations in fuel flow capacity were not substantially alleviated. The observed constraints were exclusively linked to the physical configuration of the distributor, particularly its restricted cross-sectional area, which ultimately acted as the principal bottleneck. To fully enable the utilisation of low-LHV fuels, a redesign of the fuel distribution hardware is therefore essential. Importantly, such modifications remain relatively straightforward to implement within the current system architecture, which marks a clear advantage compared to the previous setup, where no possible adjustment could solve this problem.

From the perspective of control, however, the developed fuel supply system architecture, supported by the reprogrammed ECU, proved highly successful and robust across all tested fuels. The ECU updates consistently ensured precise calculation of fuel delivery, effective idle stabilisation, and reliable torque or speed control via CAN bus, thereby validating the control strategies implemented in this project. Taken together, these findings demonstrate that it is technically feasible to adapt an existing heavy-duty engine for operation on pyrolysis gas across a broad composition spectrum while maintaining high efficiency and low emissions. At the same time, they clearly delineate the boundary between the software, which has been successfully optimised, and the hardware, which now represents the limiting factor for further performance improvements.

7.2 Future Works

It is acknowledged that the work carried out in this thesis provides a robust foundation upon which several further developments can be built. These developments hold the potential to significantly enhance the flexibility, performance, and applicability of the adapted engine platform. From the control standpoint, the updated ECU software and the implemented strategies for idle stabilisation, torque control, and fuel delivery were validated across all tested fuels, confirming that the control architecture functions as intended. The principal limitation identified was therefore not related to the software or the implemented strategies, but to the geometric restrictions of the fuel distributor, which constrained operation with low-LHV syngas. A redesign of this component to allow higher mass flow rates is thus considered imperative for fully exploiting the potential of such fuels.

Expanding the testing programme to include transient load scenarios would also be highly valuable, as it would provide insights into dynamic response and real-world emission behaviour, aspects that cannot be fully captured under steady-state operation. In addition, the integration of exhaust aftertreatment systems should be considered, especially for methane-rich fuels, where elevated NO_x emissions remain difficult to mitigate solely through in-cylinder approaches. Finally, endurance testing under long-duration continuous operation is strongly recommended to evaluate mechanical wear, deposit formation, and the overall robustness of both the control architecture and the upgraded fuel delivery hardware.

References

[1] John Heywood. *Internal Combustion Engine Fundamentals 2E*. McGraw-Hill Education, 2019. ISBN: 978-1-260-11611-3.

[2] Ahmad Fayyazbakhsh et al. "Engine emissions with air pollutants and greenhouse gases and their control technologies". In: *Journal of Cleaner Production* 376 (2022). DOI: 10.1016/j.jclepro.2022.134260.

[3] "Emissions Trends and Drivers". In: *Climate Change 2022 - Mitigation of Climate Change*. 2023, pp. 215–294. ISBN: 978-1-009-15792-6. DOI: 10.1017/9781009157926.004.

[4] Muhammed Hafis et al. "A review on alternative fuels: Spray characteristics, engine performance and emissions effect". In: *Sustainable Futures* 9 (2025). DOI: 10.1016/j.sftr.2025.100456.

[5] Prabir Basu. *Biomass gasification and pyrolysis: practical design and theory*. Academic press, 2010. ISBN: 978-1-84973-102-7.

[6] Martin Tunér. *Combustion of Alternative Vehicle Fuels in Internal Combustion Engines*. Tech. rep. Lund University, Department of Energy Sciences, Division of Combustion Engines, 2015. URL: https://www.lth.se/fileadmin/kcfp/SICEC/f3SICEC_Delrapport2_Combustion_final.pdf.

[7] EigenPlus. *Four Stroke Engine: Construction, Working, and Limitations*. Accessed: 2025-02-21. 2025. URL: https://www.eigenplus.com/four-stroke-engine-construction-working-limitations/.

[8] Richard Stone. *Introduction to Internal Combustion Engines*. Society of Automotive Engineers, 1999. ISBN: 9780768020847.

[9] Manuel I González. "Experiments with eddy currents: the eddy current brake". In: *European Journal of Physics* 25 (2004). DOI: 10.1088/0143-0807/25/4/001.

[10] European Parliament. *EU Regulation on Euro 7 Emissions Standards*. URL: https://www.europarl.europa.eu.

[11] Water Environment Federation. *Internal Combustion Engines for CHP Applications*. Tech. rep. Water Environment Federation, 2017. URL: https://www.wef.org/globalassets/assets-wef/direct-download-library/public/03---resources/wsec-2017-tr-002-rbc-internal-combustion-engines---9.2017.pdf.

[12] Saint Joseph University (ESIB), Beirut 2753, Lebanon and Chawki Lahoud. "Review of cogeneration and trigeneration systems". In: *African Journal of Engineering Research* 6 (2018). DOI: 10.30918/ajer.63.18.016.

[13] U.S. Department of Energy. *Combined Heat and Power Technology Fact Sheet: Reciprocating Engines*. URL: https://betterbuildingssolutioncenter.energy.gov/resources/combined-heat-and-power-technology-fact-sheet-reciprocating-engines.

[14] U.S. Environmental Protection Agency. *Catalog of CHP Technologies: Section 2. Technology Characterization – Reciprocating Internal Combustion Engines*. Tech. rep. U.S. Environmental Protection Agency, 2015. URL: https://www.epa.gov/sites/default/files/2015-07/documents/catalog_of_chp_technologies_section_2._technology_characterization_-_reciprocating_internal_combustion_engines.pdf.

[15] R. Bamsey. *Cogeneration: A Comprehensive Guide to CHP Systems*. McGraw-Hill, 2004.

[16] Allen J Wood, Bruce F Wollenberg, and Gerald B Sheblé. *Power generation, operation, and control*. John wiley & sons, 2013. ISBN: 9781118733868.

[17] S. Filizadeh. *Electric Machines and Drives: Principles, Control, Modeling, and Simulation*. CRC Press, 2013. ISBN: 9781315169651.

[18] Leonard L Grigsby. *Power system stability and control*. CRC press, 2007. ISBN: 9780429129728.

[19] Rasmus Lund and Brian Vad Mathiesen. "Large combined heat and power plants in sustainable energy systems". In: *Applied Energy* 142 (2015). DOI: 10.1016/j.apenergy.2015.01.013.

[20] M Godoy Simões and Felix A Farret. *Modeling and analysis with induction generators*. CRC Press, 2014. ISBN: 9781482244700.

[21] Amin Paykani et al. "Synthesis gas as a fuel for internal combustion engines in transportation". In: *Energy* 47 (2012).

[22] Maria Puig-Arnavat, Joan Carles Bruno, and Alberto Coronas. "Review and analysis of biomass gasification models". In: *Renewable and Sustainable Energy Reviews* 14 (2010). DOI: 10.1016/j.rser.2010.07.030.

[23] Anil Singh Bika. "A DISSERTATION SUBMITTED TO THE FACULTY OF THE GRADUATE SCHOOL OF THE UNIVERSITY OF MINNESOTA". en. In: ().

[24] E.V. Jithin et al. "A review on fundamental combustion characteristics of syngas mixtures and feasibility in combustion devices". In: *Renewable and Sustainable Energy Reviews* 146 (2021). DOI: 10.1016/j.rser.2021.111178.

[25] Dharmendra D. et all. Sapariya. "A review on thermochemical biomass gasification techniques for bioenergy production". In: *Energy Sources, Part A: Recovery, Utilization, and Environmental Effects* (2021). DOI: 10.1080/15567036.2021.2000521.

[26] Yuchen Gao et al. "A review of recent developments in hydrogen production via biogas dry reforming". In: *Energy Conversion and Management* 171 (2018). DOI: 10.1016/j.enconman.2018.05.083.

[27] Bjørn Christian Enger, Rune Lødeng, and Anders Holmen. "A review of catalytic partial oxidation of methane to synthesis gas with emphasis on reaction mechanisms over transition metal catalysts". In: *Applied Catalysis A: General* 346 (2008). DOI: 10.1016/j.apcata.2008.05.018.

[28] Amin Paykani et al. "Synthesis gas as a fuel for internal combustion engines in transportation". In: *Progress in Energy and Combustion Science* 90 (2022). DOI: 10.1016/j.pecs.2022.100995.

[29] Samira Lotfi. “Technologies for Tar Removal from Biomass-Derived Syngas”. In: *Petroleum & Petrochemical Engineering Journal* 5 (2021). DOI: 10.23880/ppej-16000271.

[30] Aleksander Krótki et al. “Performance Evaluation of Pressure Swing Adsorption for Hydrogen Separation from Syngas and Water–Gas Shift Syngas”. In: *Energies* 18 (2025). DOI: 10.3390/en18081887.

[31] Weikuo Zhang et al. “Effect of Hydrogen-Rich Fuels on Turbulent Combustion of Advanced Gas Turbine”. In: *Journal of Thermal Science* 31 (2022). DOI: 10.1007/s11630-021-1539-8.

[32] Fanbin Meng et al. “Emission characteristics of vehicles fueled by hydrogen-enriched syngas under no-load condition”. In: *International Journal of Hydrogen Energy* 45 (2020). DOI: 10.1016/j.ijhydene.2019.02.007.

[33] Lorenzo Menin et al. “Biomass Derived Combined Heat and Power from Decentralized Small-Scale Gasification: Updated Cost Conditions for the Italian Mountain Context and Competitiveness in Future Energy Markets”. In: *Waste and Biomass Valorization* (2025). DOI: 10.1007/s12649-025-02948-3.

[34] Laurene Desclaux and Amaro Olimpio Pereira. “Residual Biomass Gasification for Small-Scale Decentralized Electricity Production: Business Models for Lower Societal Costs”. In: *Energies* 17 (Apr. 2024). DOI: 10.3390/en17081868.

[35] Ahmed M. Salem, Harnek S. Dhami, and Manosh C. Paul. “Syngas Production and Combined Heat and Power from Scottish Agricultural Waste Gasification—A Computational Study”. In: *Sustainability* 14 (2022). DOI: 10.3390/su14073745.

[36] Walter Bohl and Werner Elmendorf. *Technische Strömungslehre*. Vieweg+Teubner Verlag / Springer Vieweg, 2013. ISBN: 978-3-8343-3329-2.

[37] Philip M. Gerhart, Andrew L. Gerhart, and John I. Hochstein. *Munson, Young and Okiishi’s Fundamentals of Fluid Mechanics*. John Wiley & Sons, 2017. ISBN: 978-1-119-54799-0.

[38] MAN Engines. *Powerful Gas Engines*. Technical brochure, Accessed: June 2025. 2023. URL: https://www.man.eu/ntg_media/media/en/content_medien/doc/man_engines_1/produkte/power_1/MAN_Engines_Power_Gas_2023_de_screen.pdf.

[39] INNIO Jenbacher. *JENBACHER Type 2 – J208 Gas Engine*. Accessed: June 2025. 2024. URL: https://www.jenbacher.com/en/gas-engines/type-2/j208.

Appendix A

Component Drawings

This appendix presents the drawings of the main components needed to mount the system used in the work. Some of them were already fabricated while others underwent changes.

PARTS LIST			
ITEM	QTY	PART NUMBER	DESCRIPTION
1	1	2101_134_432C_F_HOUSING	
2	1	2101_134_433B_F_WELLE_ANTRIEB	
3	1	2101_134_437B_F_RITZEL	
4	1	2101_134_450A_F_PLUG	
5	1	2101_134_447A_F_SCHIEBER	
6	1	2101_134_451A_F_KUGEL	
7	1	2101_134_434B_F_ROTORWELLE	
8	1	2101_134_463C_F_WELLE_HEX	
9	1	1910_134_053A_F_VPLATTE	
10	1	2101_134_006A_F_DICHTRING	
11	1	2101_134_444A_F_SCHIEBEMUFFE	
12	1	2101_134_436B_F_ZAHNRAD	
13	1	2101_134_464A_F_FLANSCH	
14	1	2101_134_446B_F_LAGER	
15	1	2101_134_465A_F_ZYLINDER	
16	1	2101_134_461C_F_LOCHPLATTE	
17	1	2101_134_445D_F_DECKEL	
18	1	2101_134_462C_F_DREHSCHIEBER	
19	1	2101_134_476A_F_STOPFEN	

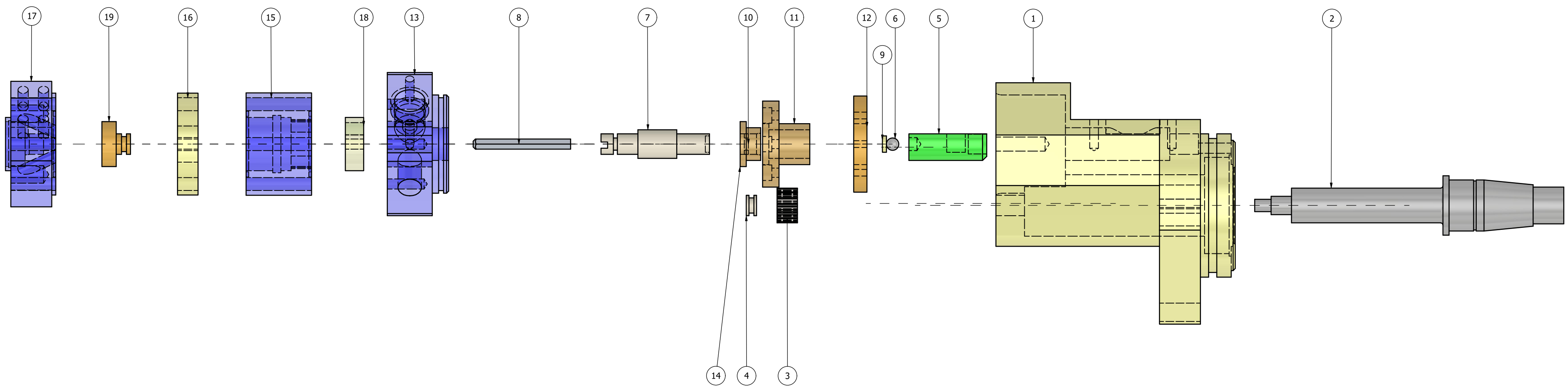

DRAWN Afonso Santos	28/07/2025			
CHECKED		TITLE		
QA		Distributor exploded view		
MFG				
APPROVED		SIZE D	DWG NO 134_430g_z_inj_verteiler	REV 1
		SCALE 1 : 1	SHEET 1 OF 1	

PARTS LIST

ITEM	QTY	PART NUMBER	DESCRIPTION
1	1	2101_134_452A_F_AKTUATOR	
2	1	2101_134_458B_F_ZYLINDER	
3	1	2101_134_479A_F_DECKEL	
4	1	2101_134_478C_F_WELLE	
5	1	2101_134_006A_F_DICHTRING	
6	1	2101_134_483B_F_MITNEHMER	
7	1	2101_134_484A_F_MEMBRANFEDER	
8	1	2101_134_480B_F_DREHSCHIEBER	
9	3	DIN2098_D-055_L1_FEDER	
10	1	ISO4017_5X30_BOLT	
11	4	ISO4762_5X100_BOLT	
12	1	SS-12M0-1-8RS-SWAGELOK COMPANY-3	
13	1	SS-12M0-1-4RS	

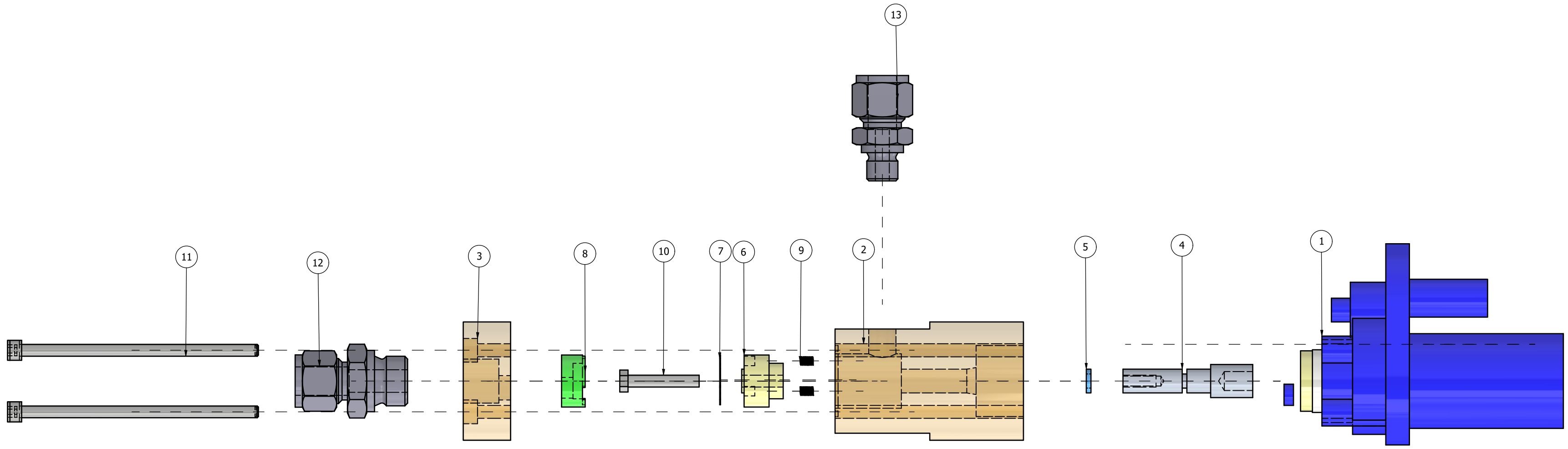

DRAWN Afonso Santos	21/07/2025		
CHECKED		TITLE	
QA		Proportional valve exploded view	
MFG			
APPROVED			
		SIZE D	DWG NO 134_457c_z_propventil	REV 1
		SCALE 1 : 1	SHEET 1 OF 1

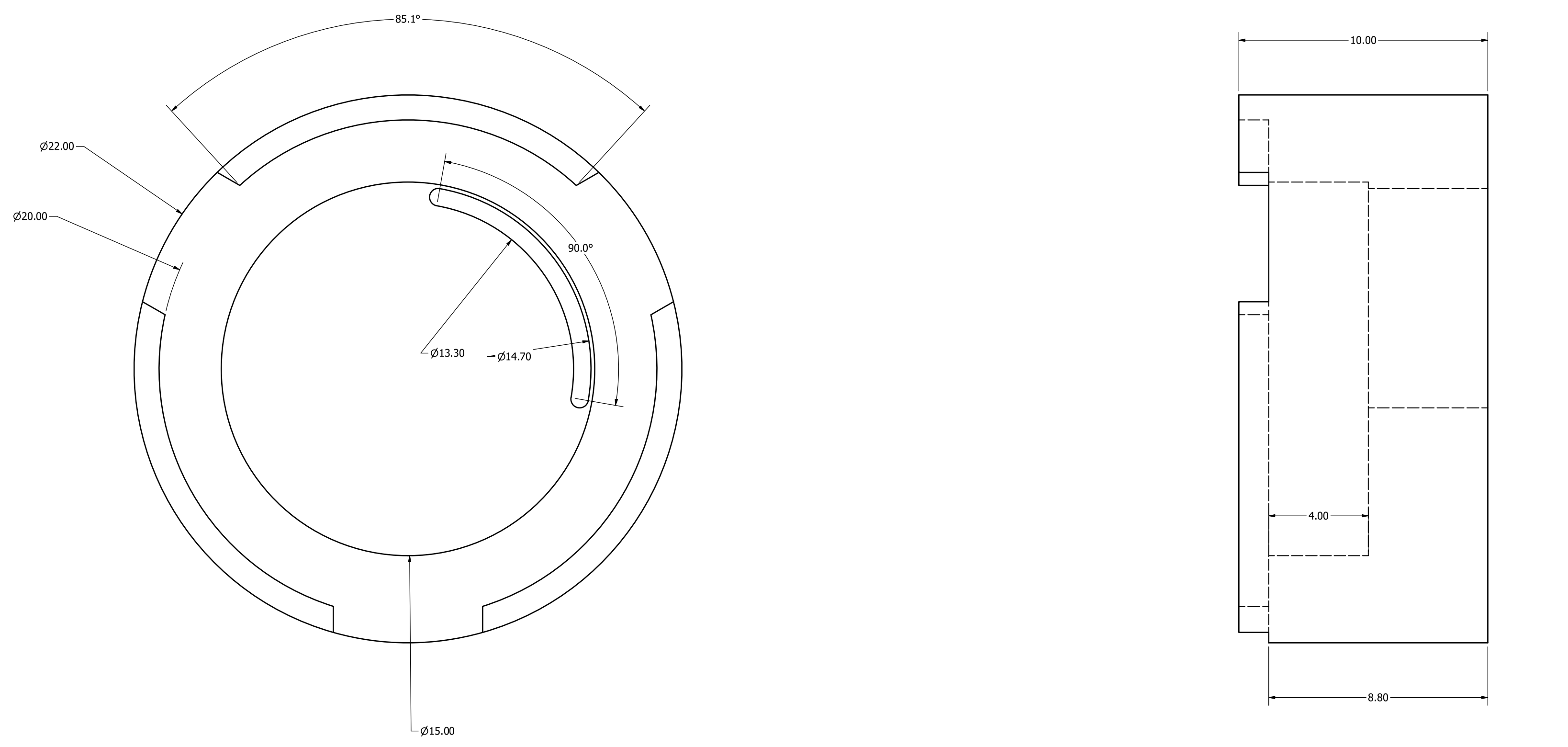

DRAWN Afonso Santos	21/07/2025	
CHECKED		TITLE
QA		Updated graphite disk
MFG		
APPROVED		SIZE D · DWG NO 134_480b_f_drehschieber · REV 1
		SCALE 10 : 1 · SHEET 1 OF 1

Appendix B

Fraunhofer Based Fuels

The present Appendix details the composition of the syngases utilised in this study. The properties of the base fuel used for the project is presented in Table B.1. The most relevant properties used for design purposes are presented in Table B.2.

Table B.1: Volumetric, Massic and Energetic Fractions of Each Constituent in Base Syngas

Species	y_i	w_i	e_i
H_2	0,29	0,03	0,26
CO_2	0,27	0,51	0,00
CO	0,29	0,35	0,29
CH_4	0,15	0,11	0,45

Table B.2: Characterisation of Base Syngas Constituents and Final Mixture

Species	M_i [kg/kmol]	γ [-]	lhv_i [MJ/kg]	ρ [kg/m^3]
H_2	2	1,41	120	0,09
CO_2	44	1,30	0,00	1,96
CO	28	1,40	10,10	1,25
CH_4	16	1,32	50,01	0,71
Syngas	22,76	1,34	12,11	1,02

Additionally, other mixtures were created by adding H_2 to the reference fuel. The compositions used for testing are presented in Table B.3.

Table B.3: Volumetric Fractions of Each Constituent in Tested Fuels

Species	S1	S2	S3
H_2	0,81	0,59	0,39
CO_2	0,07	0,16	0,23
CO	0,08	0,16	0,25
CH_4	0,04	0,09	0,13

Appendix C

Previous Setup Results

In this Appendix, the results obtained with the previous setup are presented in Figures C.1 and C.2, serving as a reference for evaluating the new setup.

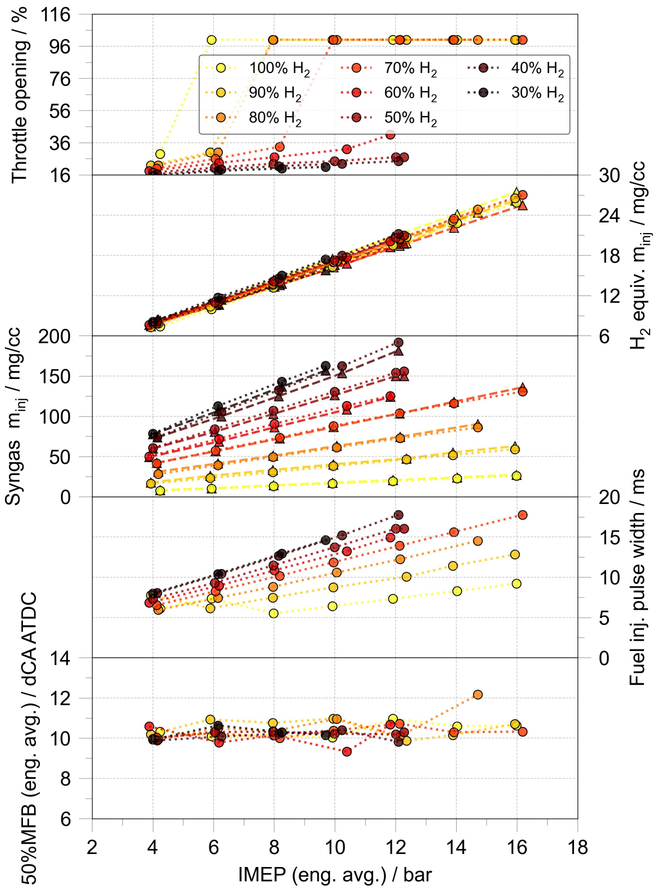

Figure C.1: Fuel supply assessment.

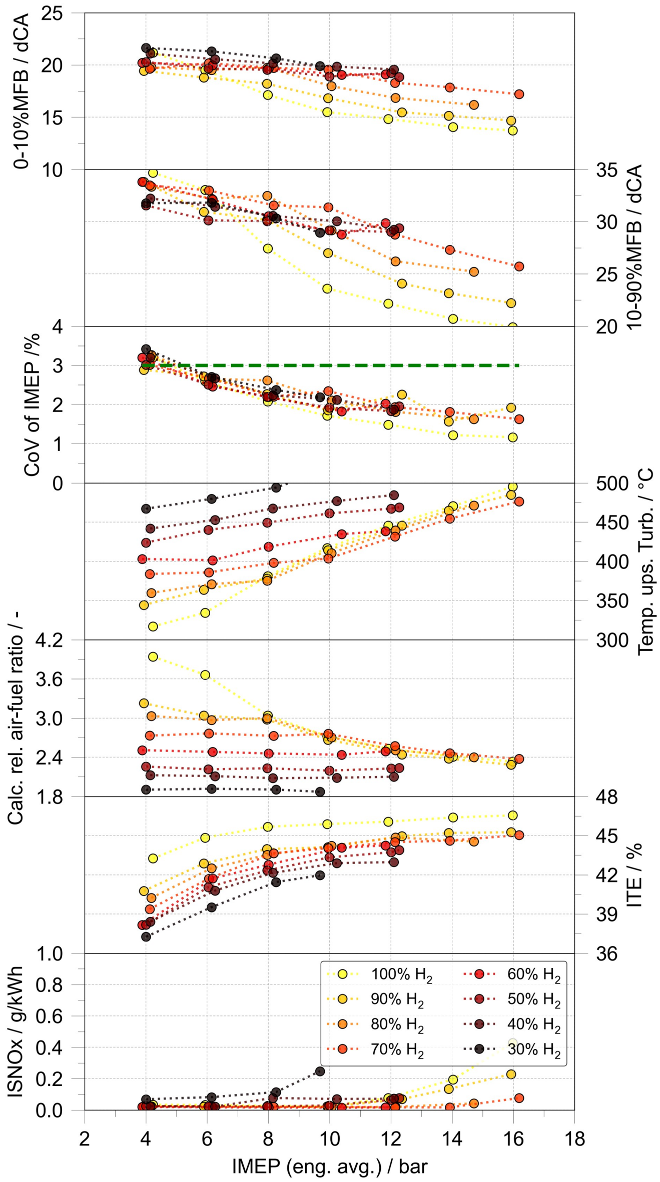

Figure C.2: Engine Output.